

# Subduction initiation during collision-induced subduction transference: Numerical modeling and implications for the Tethyan evolution

Xinyi Zhong<sup>1</sup> and Zhong-Hai Li<sup>1</sup>

<sup>1</sup>University of Chinese Academy of Sciences

November 22, 2022

## Abstract

The collision-induced subduction transference is a composite dynamic process including both the terrane collision/accretion and the subduction initiation (SI) at the neighboring passive margin. This process occurred repeatedly during the evolution of Tethyan systems, with multiple ribbon-like continents or micro-continents drifting from Gondwana in the southern hemisphere and accreting to the Eurasian continent since Paleozoic. In the previous numerical studies, the dynamics of terrane collision and induced SI are investigated individually, which however need to be integrated to study the controlling factors and time scales of collision-induced subduction transference. Systematic numerical models are conducted with variable properties of converging plates and different boundary conditions. The model results indicate that the forced convergence, rather than pure free subduction, is required to trigger and sustain the SI at the neighboring passive margin after terrane collision. In addition, a weak passive margin can significantly promote the occurrence of SI, by decreasing the required boundary force to reasonable value of plate tectonics. The lengths of subducted oceanic slab and accreting terrane play secondary roles in the occurrence of SI after collision. Under the favorable conditions of collision-induced subduction transference, the time required for SI after collision is generally short within 10 Myrs, which is consistent with the general geological records of Cimmerian collision and the following Neo-Tethyan SI. In contrast, the stable Indian passive margin and absence of SI in the present Indian Ocean may due to the low convergent force and/or the lack of proper weak zones, which remains an open question.

## Hosted file

collision-induced subduction zone transference\_4\_sp.docx available at <https://authorea.com/users/534711/articles/598545-subduction-initiation-during-collision-induced-subduction-transference-numerical-modeling-and-implications-for-the-tethyan-evolution>

1     **Subduction initiation during collision-induced subduction transference: Numerical**  
2                     **modeling and implications for the Tethyan evolution**

3  
4                     **Xinyi Zhong<sup>1</sup>, Zhong-Hai Li<sup>1\*</sup>**

5     <sup>1</sup> Key Laboratory of Computational Geodynamics, College of Earth and Planetary Sciences,  
6     University of Chinese Academy of Sciences, Beijing 100049, China.

7  
8     Corresponding author: Z.-H. Li (li.zhonghai@ucas.ac.cn)

9  
10  
11  
12  
13     **Key Points:**

- 14             • Forced convergence is required for the collision-induced subduction transference which  
15             generally occurs within 10 Myrs after collision.
- 16             • The weakness of passive margin significantly promotes subduction initiation after the  
17             terrane collision and accretion.
- 18             • The collision-induced subduction initiation of Neo-Tethyan plate may indicate large  
19             convergent force and/or weakened passive margin.
- 20

21 **Abstract**

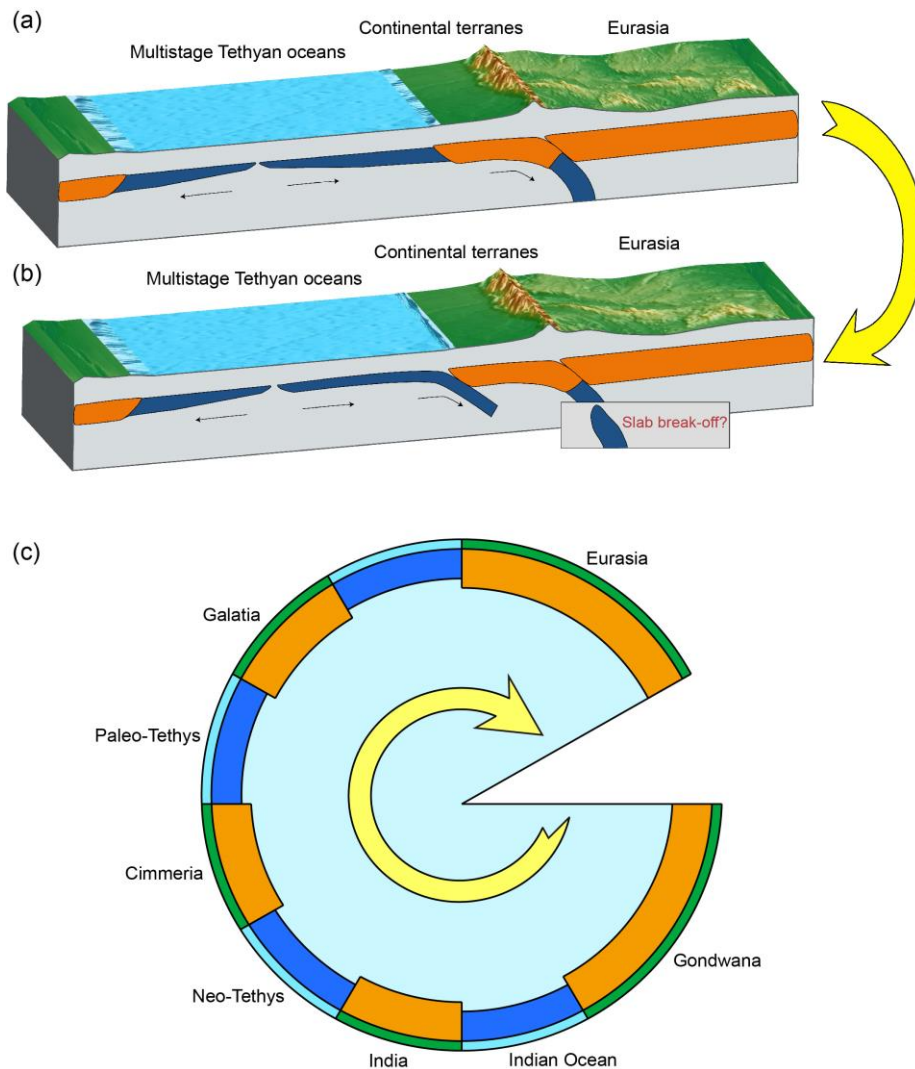
22         The collision-induced subduction transference is a composite dynamic process including  
23 both the terrane collision/accretion and the subduction initiation (SI) at the neighboring passive  
24 margin. This process occurred repeatedly during the evolution of Tethyan systems, with multiple  
25 ribbon-like continents or micro-continents drifting from Gondwana in the southern hemisphere  
26 and accreting to the Eurasian continent since Paleozoic. In the previous numerical studies, the  
27 dynamics of terrane collision and induced SI are investigated individually, which however need  
28 to be integrated to study the controlling factors and time scales of collision-induced subduction  
29 transference. Systematic numerical models are conducted with variable properties of converging  
30 plates and different boundary conditions. The model results indicate that the forced convergence,  
31 rather than pure free subduction, is required to trigger and sustain the SI at the neighboring  
32 passive margin after terrane collision. In addition, a weak passive margin can significantly  
33 promote the occurrence of SI, by decreasing the required boundary force to reasonable value of  
34 plate tectonics. The lengths of subducted oceanic slab and accreting terrane play secondary roles  
35 in the occurrence of SI after collision. Under the favorable conditions of collision-induced  
36 subduction transference, the time required for SI after collision is generally short within 10 Myrs,  
37 which is consistent with the general geological records of Cimmerian collision and the following  
38 Neo-Tethyan SI. In contrast, the stable Indian passive margin and absence of SI in the present  
39 Indian Ocean may due to the low convergent force and/or the lack of proper weak zones, which  
40 remains an open question.

41

42

## 43 1 Introduction

44 In the plate tectonics and Wilson's cycle, the plate convergence starts with the subduction  
 45 initiation (SI) and terminates with the continental collision and orogeny. Because of the low  
 46 density of continental crust, the continental subduction-collision process cannot last for very long  
 47 time as the oceanic subduction. Thereby, the plate convergence will generally stop after the  
 48 orogeny with a timescale of several tens of million years, although the special case of India-Asia  
 49 collision is still ongoing after ~50 Ma (*Yin and Harrison, 2000; Aitchison et al., 2007; Najman,*  
 50 *et al., 2010; DeCelles et al., 2014; Zhu et al., 2015*). On the other hand, with the collision of a  
 51 buoyant block, a new subduction zone may form in the neighboring plate to accommodate the  
 52 continuous convergence, which is defined as the 'collision-induced subduction transference'  
 53 (Figure 1a, b) (*Niu et al., 2003; Stern, 2004; Zhu et al., 2011; Stern and Gerya, 2018*). It may  
 54 play a crucial role in the accretion and amalgamation of continents (*Stern, 2017*).



55  
56

57 **Figure 1.** The conceptual sketch of repeated subduction initiation during collision-induced  
 58 subduction transference and accretion of multiple continental terranes with Eurasian continent  
 59 throughout the Tethyan evolution. (a) Collision of the continental terranes with Eurasia. (b)

60 Subduction initiation at the neighboring passive margin. (c) Multiple subduction-collision-  
61 subduction processes during the evolution of Tethyan system.

62

63 The collision-induced subduction transference, although without clear Cenozoic  
64 examples, is quite popular in the evolution of Tethyan system, which experienced multiple  
65 subduction-collision-subduction processes, as well as the assembly or accretion of terranes  
66 (Figure 1c) (Şengör, 1988; Stampfli and Borel, 2002; Zhu et al., 2011, 2013; Metcalfe, 2013;  
67 Wan et al., 2019). The ribbon-like continents or micro-continents continuously drifted from  
68 Gondwana in the southern hemisphere and accreted to the Eurasian continent throughout the  
69 evolution of the Tethyan system since Paleozoic (Figure 1c). The Tethyan system began with the  
70 breakup of the Galatian super terrane from the Gondwana, resulting in the opening of Paleo-  
71 Tethyan Ocean. The collision between the Galatian terrane and Laurasia finally closed the Rheic  
72 Ocean, with the subduction transferred to the Paleo-Tethys (Stampfli et al., 2013). Then, the  
73 Cimmerian terranes broke up from the Gondwana in late Paleozoic, leading to the opening of  
74 Neo-Tethyan Ocean. The collision of the Cimmerian terranes with Laurasia closed the Paleo-  
75 Tethys, after which the subduction was transferred to the Neo-Tethys in Mesozoic (Stampfli and  
76 Borel, 2002; Zhu et al., 2013; Wan et al., 2019). Finally, the Indian plate broke up from  
77 Gondwana in Cretaceous and collided with the Eurasian plate at around 55 Myrs (Yin and  
78 Harrison, 2000; Aitchison et al., 2007; Najman, et al., 2010; DeCelles et al., 2014; Zhu et al.,  
79 2015; Searle, 2019). Although the collision has lasted for a long time, there is still no clear sign  
80 for the SI in the present-day Indian Ocean (Stern, 2004; Stern and Gerya, 2018). Thus, it is still a  
81 mystery and challenge that whether and when the Indian Oceanic plate will begin subduction.

82 From the summarized Tethys evolution history, a crucial issue for the continuous plate  
83 convergence is the SI after the terrane collision and accretion, i.e. the collision-induced  
84 subduction transference (Figure 1a, b). Its dynamics is rarely investigated and thus still not  
85 resolved. The previous correlated numerical studies are generally focusing on two points. One is  
86 the subduction of anomalous blocks within an oceanic plate, including the island arc, oceanic  
87 plateaus or continental fragments, which is generally focusing on the resulting flat subduction  
88 (van Hunen et al., 2002, 2004; Mason et al., 2010) or the contrasting modes of accretion (e.g.,  
89 Selzer et al., 2008; Tetreault and Büter, 2012; Vogt and Gerya, 2014; Yang et al., 2018).  
90 Notably, a ‘trench jump’ after collision is predicted in some of the models (Tetreault et al., 2012;  
91 Vogt and Gerya, 2014; Yang et al., 2018), which is however caused by the detachment of weak  
92 and buoyant crust of the accreting terrane, rather than initiating a new subduction zone in the  
93 neighboring oceanic plate. Another type of model focuses on the SI at passive continental  
94 margins, which only deal with two plates and a transition between them (e.g., Toth and Gurnis,  
95 1998; Nikolaeva et al., 2011; Rey et al., 2014; Baes and Sobolev, 2017; Zhong and Li, 2019;  
96 Ulvrova et al., 2019). These models indicate that the SI at passive continental margin is not easy,  
97 which generally requires special conditions, for example, (1) the thin, weak and very buoyant  
98 continental lithosphere (e.g., Nikolaeva et al., 2011; Marques et al., 2013, 2014; Rey et al., 2014),  
99 (2) a prescribed weak transition zone between the continental and oceanic plates (e.g. Toth and  
100 Gurnis, 1998; Baes et al., 2011), (3) driven by downward mantle flow (e.g. Baes and Sobolev,  
101 2017) or (4) driven by a boundary stress/force (e.g., Zhong and Li, 2019). On the other hand, the  
102 natural examples of Atlantic and Indian passive margins, neighboring to relatively old oceanic  
103 lithospheres, are generally stable and difficult for SI (Cloetingh et al., 1989; Mueller and Philips,  
104 1991, Niu et al., 2003; Stern and Gerya, 2018; Zhong and Li, 2019). Thus, it indicates that the

105 collision-induced subduction transference during Tethyan evolution should not be so easy,  
106 because the multiple Tethyan Oceans generally have an old and thick lithosphere at the passive  
107 margin (*Stampfli and Borel, 2002; Müller et al., 2008; Stampfli, 2013*). In this study, we aim to  
108 combine the models with terrane collision/accretion and SI at the passive margins, in order to  
109 understand the dynamics of collision-induced subduction transference as well as the key point of  
110 Tethyan evolution.

111 Another important issue for the collision-induced subduction transference is the time  
112 span between the terrane collision and SI in the neighboring plate. In the Tethyan system, for  
113 example, the collision of the Qiangtang-Lhasa terrane, which occurred in Early Cretaceous (~140  
114 Ma), may trigger the northward SI (~137 Ma) of the Indus-Yarlung Zangbo Tethyan ocean, i.e. a  
115 branch of the Neo-Tethys (*Zhu et al., 2013*). The time for the collision between the Iranian  
116 terrane and Eurasia was at about 228~201 Ma, whereas the neighboring SI at about 187 Ma  
117 (*Wan et al., 2019*), which indicates the SI occurring at about 20 Myrs after the collision. Notably,  
118 the times and time spans between collision and neighboring SI in Tethyan system are not well  
119 constrained due to the vague geological records. Specially, the Indian Oceanic plate does not  
120 begin subduction after the India-Eurasia collision for >50 Myrs, which makes it even more  
121 difficult to answer the question from geological observations (*Niu et al., 2003; Stern, 2004; Stern  
122 and Gerya, 2018*).

123 The required conditions and time scales of collision-induced subduction transference are  
124 rarely studied and thus remain unresolved. In order to study these problems, systematical  
125 numerical models are conducted with variable properties of converging plates and different  
126 boundary conditions. The model results are further compared with the geological records of  
127 Tethys and shed new lights on the Tethyan dynamic evolution as well as the plate tectonic theory.

128

## 129 **2 Initial Model Setup**

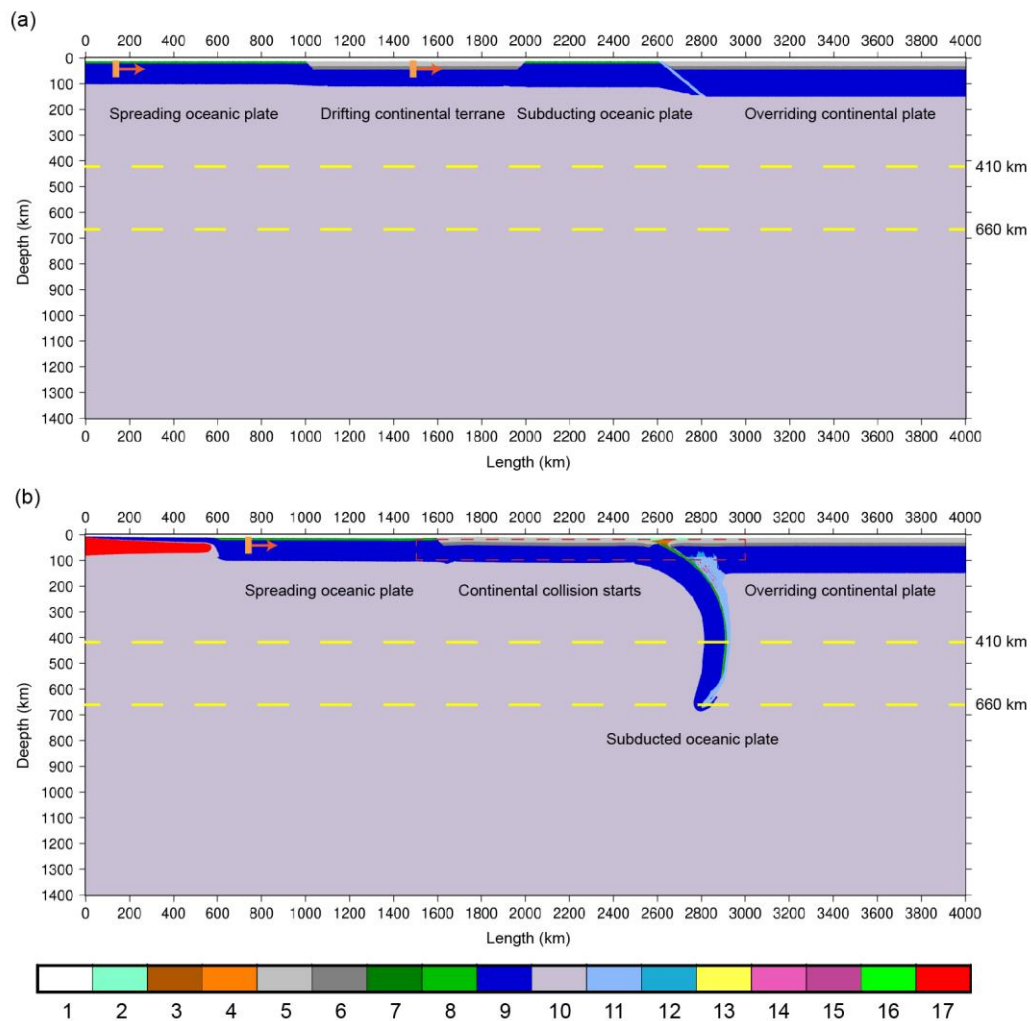
### 130 **2.1 Original model setup**

131 The 2-D original model is 4000 km in length and 1400 km in depth, as shown in Figure  
132 2a. The model includes two oceanic plates and two continental plates. A spreading oceanic plate  
133 (1000 km) is configured on the left side of the model, which is neighbored by a drifting  
134 continental terrane (1000 km). Another oceanic plate (600 km) is set between the drifting  
135 continental terrane and the overriding continental plate (1400 km). A weak zone is initially  
136 applied between the subducting oceanic plate and the overriding continental plate. Wet olivine  
137 rheology is applied for the weak zone, whereas dry olivine rheology is used for normal mantle  
138 rocks (*Karato and Wu, 1993*). The crust of continental plate is set to be 35 km, including a 20 km  
139 thick upper crust and a 15 km thick lower crust. For the drifting continental plate, the  
140 lithospheric thickness is set to be 100 km, whereas the overriding continental lithosphere is 140  
141 km thick. The oceanic lithosphere is composed of a 3 km thick basalt layer as the upper crust, a 5  
142 km thick gabbro layer as the lower crust, as well as a lithospheric mantle layer with the thickness  
143 dependent on the age (*Turcotte and Schubert, 2002*). The subducting oceanic plate is 100 km in  
144 thickness and 180 Ma in age, whereas the age of spreading oceanic plate is varied in the  
145 numerical studies. A ‘stick air’ layer is applied on the top of the model to allow the deformation  
146 of the crustal surface (*Schmeling et al., 2008; Crameri et al., 2012*). In the model, a ‘stick air’

147 layer of 10 km thick is set above the continental plate and 12 km above the oceanic plate, in  
 148 order for the gravity isostasy.

149 The temperature conditions of the top and bottom boundaries are fixed, with 273 K and  
 150 2248 K, respectively. The left and right boundaries are adiabatic, with no heat flux across them.  
 151 For the thermal structure of oceanic lithosphere, half-space cooling model is applied (e.g.,  
 152 *Turcotte and Schubert, 2002*). For the continental lithosphere, a linear temperature gradient is  
 153 applied with 273 K on the surface and 1623 K at the bottom of lithosphere. An adiabatic  
 154 temperature gradient of 0.5 K/km is applied for the sub-lithospheric mantle. The phase  
 155 transitions at 410 km and 660 km are applied (*Li et al., 2019*), with the Clapeyron slopes of 2.5  
 156 MPa/K and -1.0 MPa/K, respectively.

157 All the velocity boundary conditions of the model are set to be free slip. The subducting  
 158 plate is pushed with a constant velocity ( $v_x = 10$  cm/yr) in the left side of the spreading oceanic  
 159 plate and the middle of drifting continental terrane, as shown in Figure 2a with two orange  
 160 rectangles and arrows. The same constant convergent velocities are applied for 6 Myrs in the  
 161 original model in order to avoid deformation in the passive margin between spreading oceanic  
 162 plate and drifting continental plate.



164 **Figure 2. (a)** Original model configuration with an overriding continental plate, a subducting  
165 oceanic plate and an initial weak zone in between. Wet olivine rheology is applied for the weak  
166 zone, whereas dry olivine rheology is used for normal mantle rocks (*Karato and Wu, 1993*). A  
167 drifting continental terrane is incorporated in the oceanic plate. The subducting plate is pushed at  
168 two different positions as marked by the orange rectangles and arrows, with the same and  
169 constant velocity ( $v_x = 10$  cm/yr). **(b)** The beginning of continental collision after 6 Myrs with  
170 total convergence of 600 km. This snapshot is used as the initial model for the following study,  
171 which is either pure free subduction without any pushing, or pushed by a constant force at the  
172 left tip of the spreading oceanic plate. The yellow dashed lines denote the 410 km and 660 km  
173 discontinuities. Colors indicate the rock types, specified by the color grid: 1, stick air; 2, sea  
174 water; 3,4, sediments; 5,6, continental upper and lower crust, respectively; 7,8, oceanic upper  
175 and lower crust, respectively; 9, lithospheric mantle; 10, asthenosphere, 11, hydrated mantle; 12,  
176 serpentinized mantle; 13, partially molten sediments; 14, partially molten continental upper  
177 crust; 15, partially molten continental lower crust; 16, partially molten oceanic crust; 17, partially  
178 molten mantle.

179

## 180 **2.2 Model setup and boundary conditions from collision**

181 The original model in Figure 2a is pushed by a constant velocity of 10 cm/yr for 6 Myrs,  
182 with a total convergence of 600 km. It leads to a snapshot with the beginning of continental  
183 collision, as shown in Figure 2b, after which the previous boundary conditions with constant  
184 convergent velocity are cancelled. Thus, the original model driven by boundary velocity is only  
185 used for the first subduction and provides the slab pull force for the further evolution of the  
186 model.

187 In the following study, the initial collision snapshot (Figure 2b) is employed as the initial  
188 model. Two different types of boundary conditions are further applied and compared. One is the  
189 self-consistent free subduction driven purely by the slab pull, i.e. no pushing anywhere. Another  
190 one is pushed by a constant force at the left tip of the spreading oceanic plate (Figure 2b), the  
191 effect of which is combined with the slab pull from the subducted slab. The conditions for the SI  
192 of spreading oceanic plate after the continental collision will be systematically studied.

193 Detailed numerical methodologies (i.e. governing equations, rheological flow laws, phase  
194 transitions, hydration and partial melting) are shown in the supporting information and following  
195 *Li et al. (2019)*.

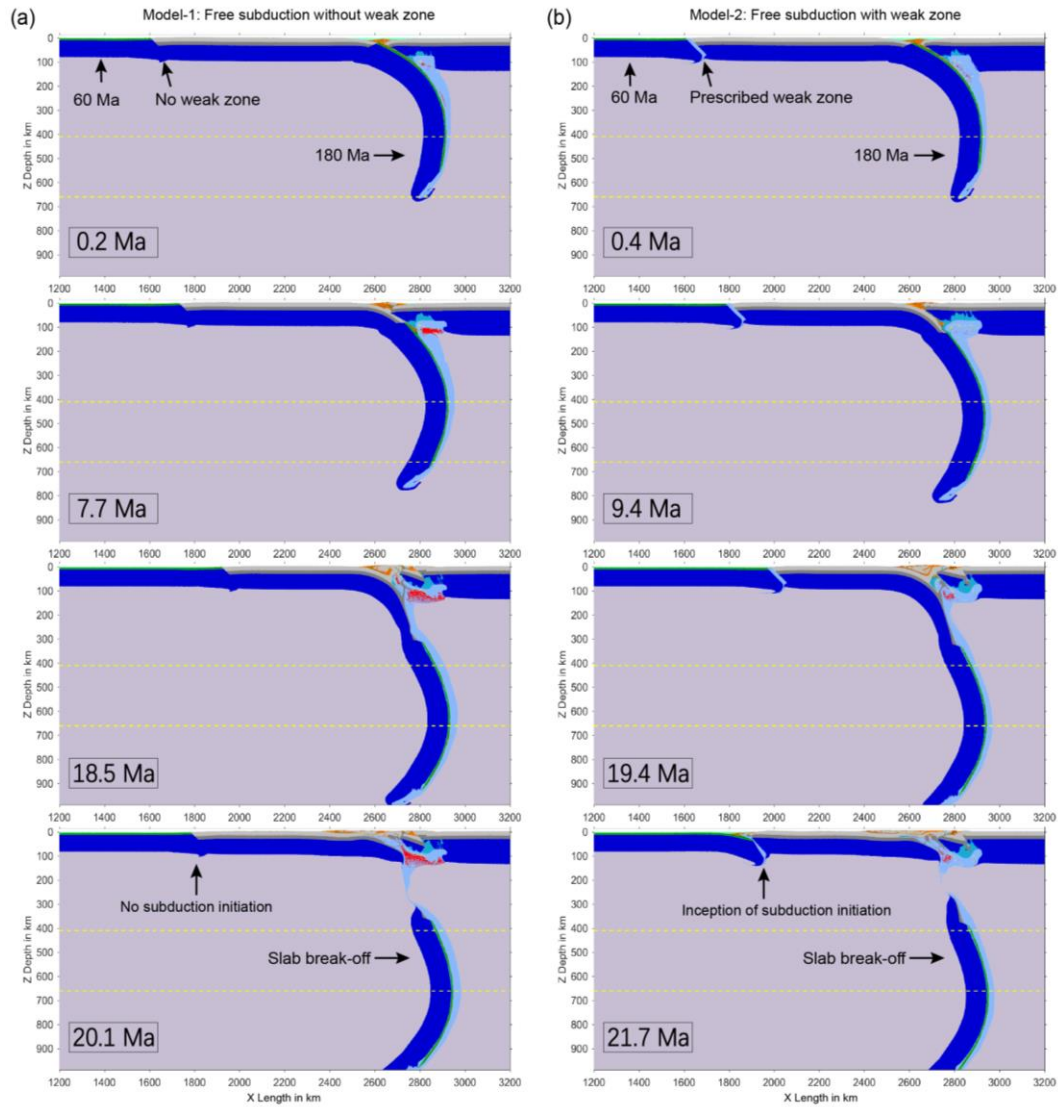
196

## 197 **3 Model Results**

### 198 **3.1 Free subduction after collision**

199 In this set of models, no prescribed convergent boundary conditions are applied after the  
200 initial collision. In order to study the collision-induced subduction transference and SI at the  
201 passive margin, two different models with contrasting rheological strengths of passive margin  
202 are applied. In Model-1, no weak zone is prescribed (Figure 3a). In Model-2, an initial weak  
203 zone with wet olivine rheology (*Karato and Wu, 1993*) is applied in the ocean-continental  
204 transition (OCT) zone (Figure 3b).

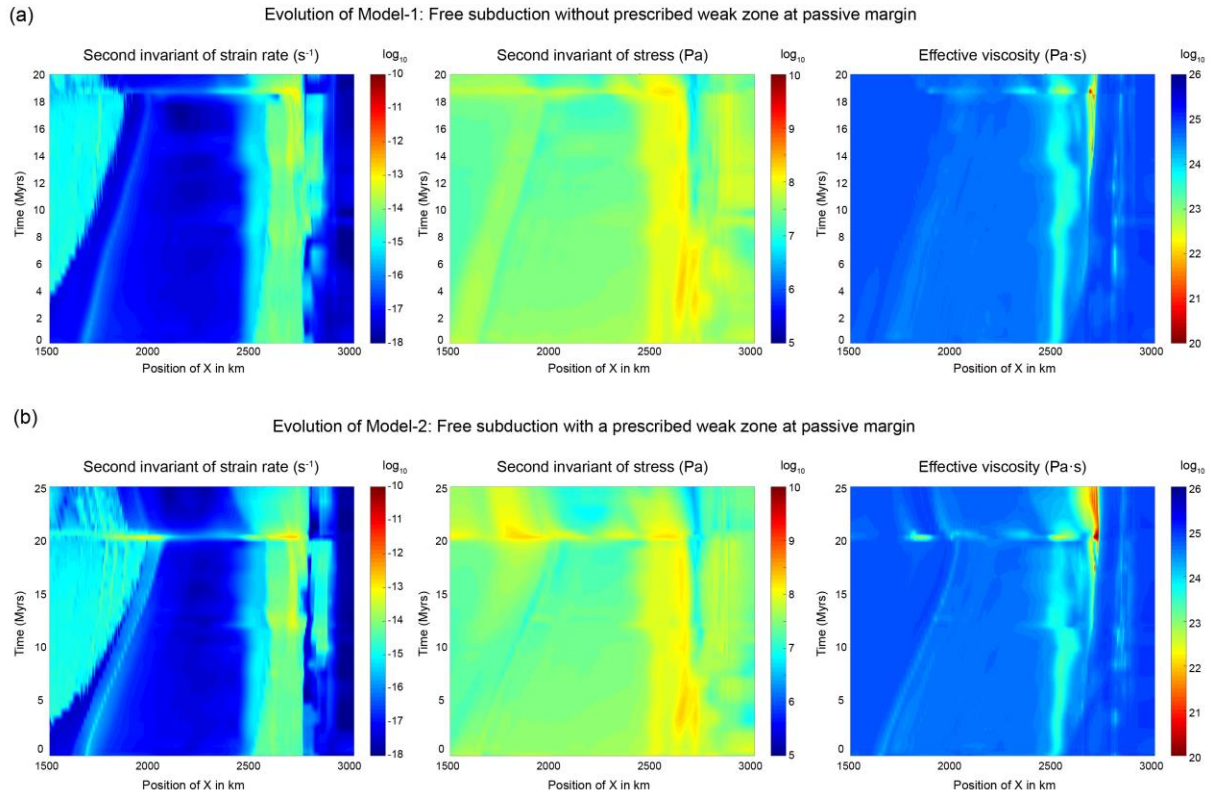
205           The evolutions of these two models are similar before the slab break-off (c.f. Figures 3a  
206 and 3b). The dehydration occurs during the previous subduction of the oceanic crust, which  
207 results in a weak subduction channel. The drifting continental lithosphere subducts under the  
208 fixed overriding continental plate, driven by the slab pull from the subducted oceanic plate.  
209 However, due to the low density, a part of the continental crust is detached and exhumed to the  
210 surface or the crustal level. Another part of continental crust could be dragged into the mantle.  
211 The buoyancy of subducted continental crust competes with the slab pull from sinking oceanic  
212 pate. Finally, the slab break-off occurs around the OCT. Consequently, the subducted continental  
213 plate migrates upward with the loss of slab pull (i.e. eduction) (*Duretz et al., 2012*), which  
214 pushes the neighboring passive continental margin and modifies the stress and strain rate fields  
215 as shown in Figures 4a and 4b. In Model-1 without any prescribed weak zone, the eduction-  
216 induced deformation is rather limited that no clear sign for SI can be observed (Figure 3a). There  
217 is no significant deformation or stress localization in the neighboring passive margin after the  
218 break-off (Figure 4a). In Model-2 with a prescribed weak zone, an incipient subduction initiates  
219 at the beginning (Figure 3b), which stops a short time later due to the limited pushing from  
220 eduction. The deformation and stress localization emerge in the neighboring passive margin  
221 corresponding to the inception of SI, which however quickly fades with time (Figure 4b). Thus,  
222 the collision-induced subduction transference is not applicable in such cases with free subduction  
223 after collision (Figure 3).



224

225 **Figure 3.** Models of free subduction after collision, with colors indicating rock types as shown in  
 226 Figure 2. (a) Evolution of Model-1 without prescribed weak zone at the passive margin. (b)  
 227 Evolution of Model-2 with a prescribed weak zone at the passive margin.

228



229

230 **Figure 4.** The time-dependent evolution of strain rate, stress and viscosity fields. The position of  
 231 the profile ( $X = 1500\sim 3000$  km) is indicated by the red box in Figure 2b, with values of second  
 232 invariant of strain rate and stress, as well as the effective viscosity averaged with depth. (a)  
 233 Evolution of Model-1 without prescribed weak zone at the passive margin, same as Figure 3a.  
 234 (b) Evolution of Model-2 with a prescribed weak zone at the passive margin, same as Figure 3b.

235

### 236 3.2 Forced subduction after collision

237 In nature, a horizontal plate without connecting to any subducting slab could also be  
 238 dragged to move by the pushing from mid-ocean ridge and shearing from the mantle convection  
 239 (*Turcotte and Schubert, 1982; Niu et al., 2003; Mahatsente, 2017; Sun, 2019*). In this section, we  
 240 conduct systematic numerical models with a constant convergent force employed on the  
 241 spreading oceanic plate (Figure 2b) to investigate the conditions and time scale of collision-  
 242 induced subduction transference. The models are classified into two groups, i.e. without or with a  
 243 prescribed weak zone at the passive margin.

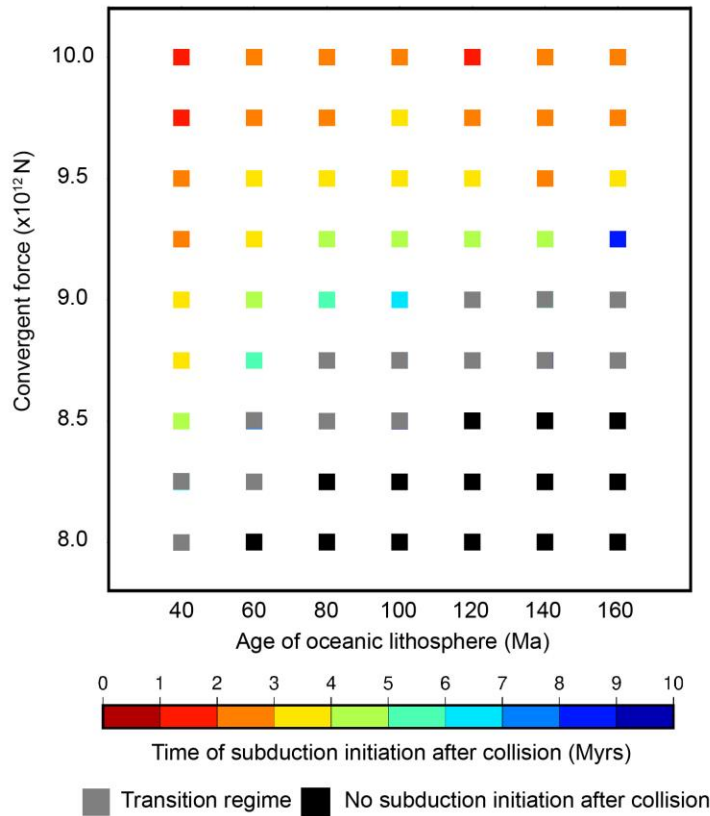
244

#### 245 3.2.1 No prescribed weak zone at the neighboring passive margin

246 Systematic numerical models are conducted with variable convergent boundary forces  
 247 and variable ages of the spreading oceanic plate (Figure 5). The model results indicate that the  
 248 collision-induced SI at the neighboring passive margin requires a relatively high boundary force,  
 249 i.e.  $>8.0 \times 10^{12}$  N/m, which slightly increases with older oceanic lithosphere. If the boundary force  
 250 is larger enough for a specific passive margin, the SI generally occurs within 10 Myrs after the

251 initial collision (Figure 5). This time scale of SI is also dependent on the boundary force, i.e. the  
 252 larger boundary force resulting in earlier SI occurrence.

253



254

255 **Figure 5.** The occurrence and time scale of subduction initiation after collision, dependent on the  
 256 convergent boundary force and the age of oceanic lithosphere.

257

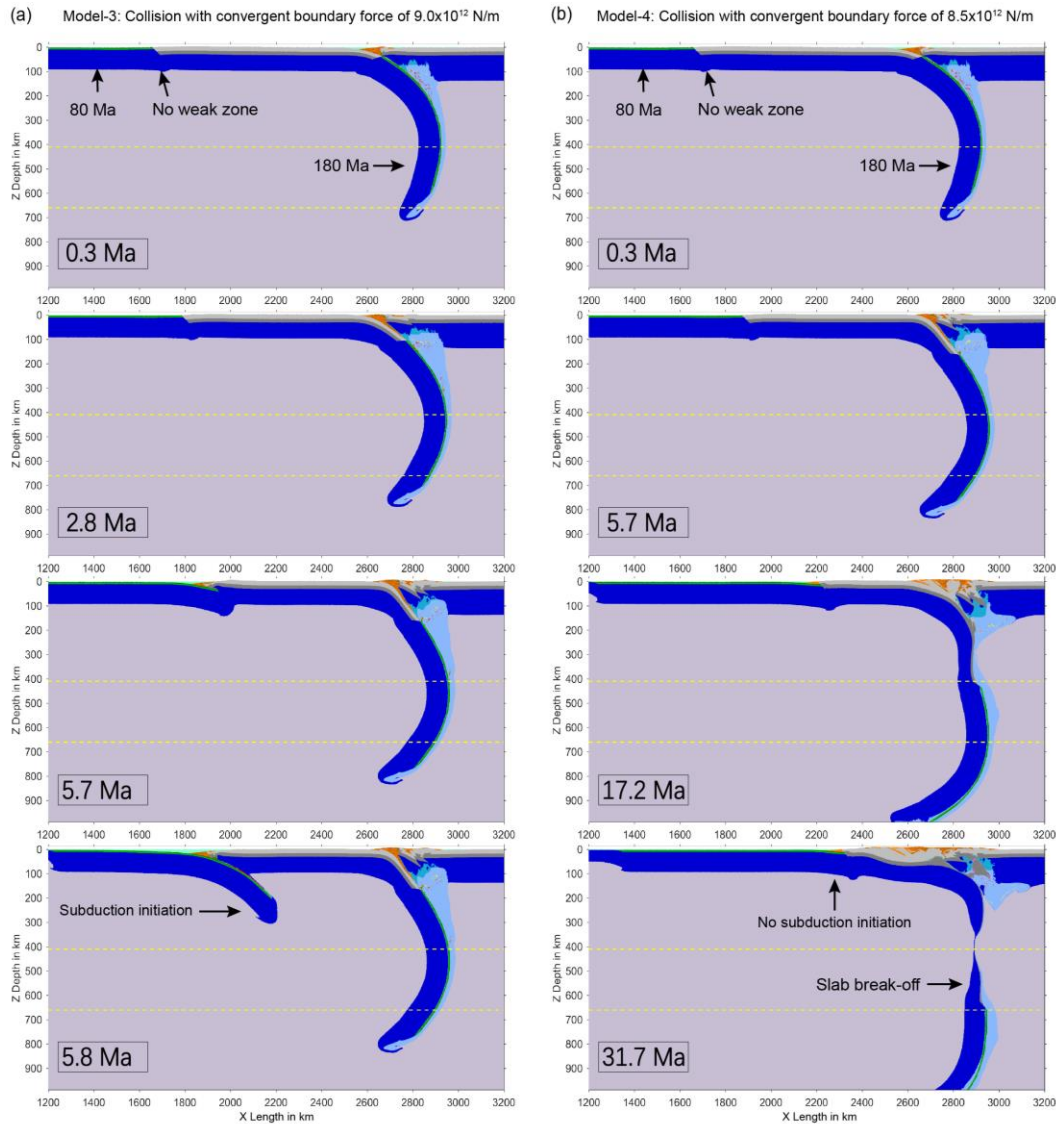
258 The detailed evolutions of two representative models are further demonstrated, i.e.  
 259 Model-3 with oceanic lithosphere of 80 Ma and boundary force of  $9.0 \times 10^{12}$  N/m, as well as  
 260 Model-4 with oceanic lithosphere of 80 Ma and boundary force of  $8.5 \times 10^{12}$  N/m (Figures 6 and  
 261 7). In Model-3, the SI occurs at the neighboring passive margin during subduction of the  
 262 continental terrane, at about 4 Myrs after initial collision. The evolution of stress field (Figure  
 263 7a) demonstrates a significant stress localization at  $X=1600-2000$  km, i.e. around the OCT in the  
 264 neighboring passive margin (Figure 6a). This process lasts for about 2 Myrs and finally leads to  
 265 SI with high strain rate and release of stress (Figure 7a).

266

267 As a comparison, the relatively low boundary force in Model-4 prevents the collision-  
 268 induced SI at the neighboring passive margin (Figure 6b). In this regime, the general stress  
 269 building occurs slowly and in a wider region, which leads to weak strain localization in the  
 270 neighboring passive margin (Figure 7b). Thus, the SI is not predicted. In more details, there are  
 271 two peak stress localization processes around the passive margin. The first one occurs at about  
 272 10 Myrs after collision, which is corresponding to the detachment and exhumation of the  
 subducted continental crust. However, it just lasts for a short time and does not result in SI. The

273 later stress localization occurs at around 30 Myrs (Figure 7b), corresponding to the slab break-  
 274 off, which again does not lead to abrupt failure of the passive margin. Finally, although the  
 275 extensive continental collision occurs for >30 Myrs, no SI is predicted at the neighboring passive  
 276 margin.

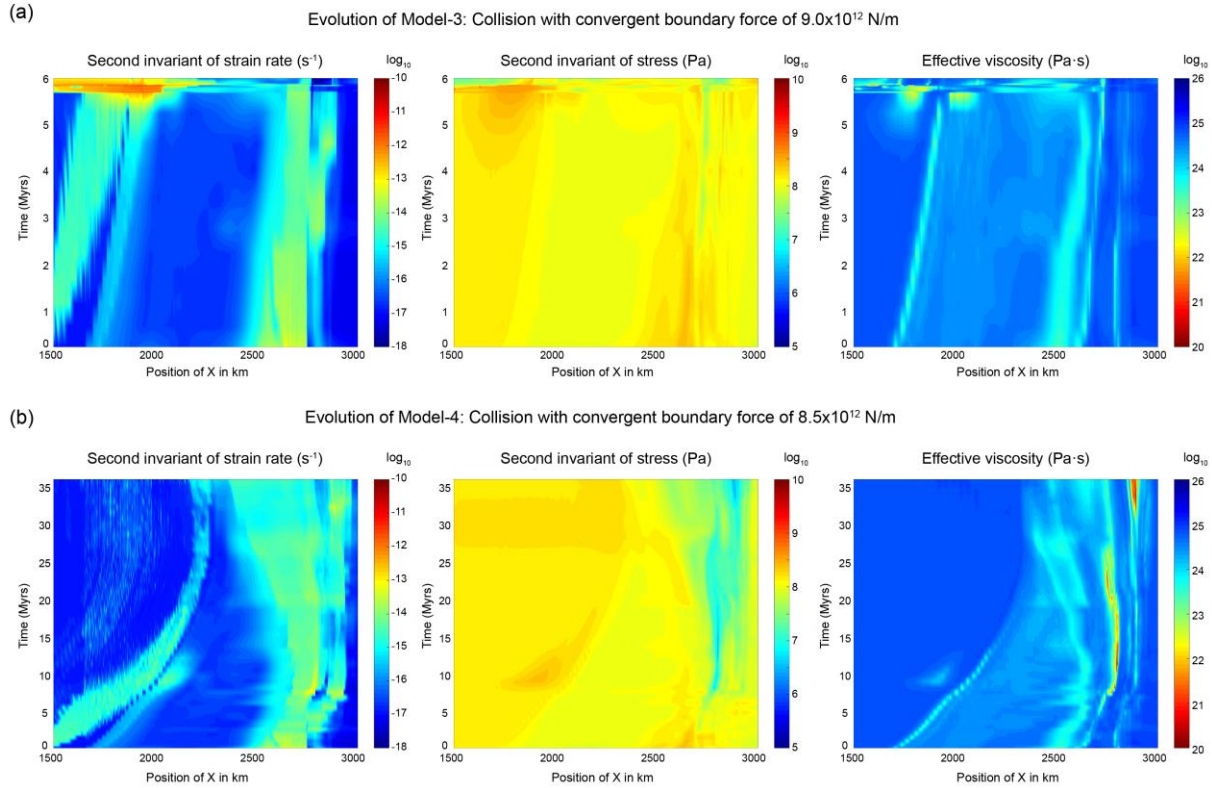
277



278

279 **Figure 6.** Models of forced subduction after collision, with colors indicating rock types as in  
 280 Figure 2. No initial weak zone is prescribed at the passive margin. (a) Evolution of Model-3 with  
 281 convergent boundary force of  $9.0 \times 10^{12}$  N/m. (b) Evolution of Model-4 with convergent  
 282 boundary force of  $8.5 \times 10^{12}$  N/m.

283



284

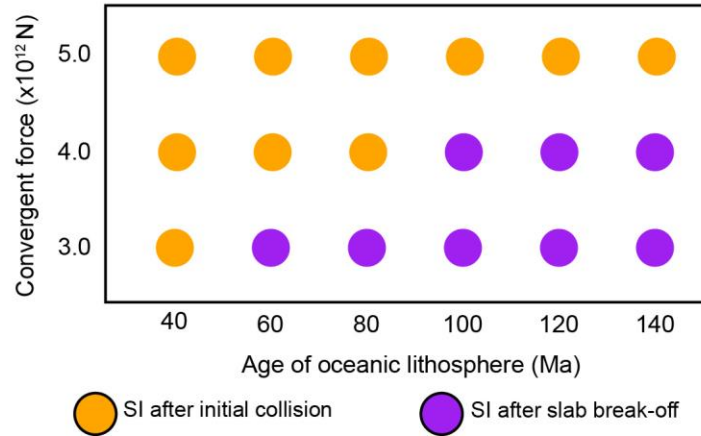
285 **Figure 7.** The time-dependent evolution of strain rate, stress and viscosity fields. The position of  
 286 the profile ( $X = 1500\sim 3000$  km) is indicated by the red box of Figure 2b, with the values of  
 287 second invariant of strain rate and stress, as well as the effective viscosity averaged with depth.  
 288 (a) Evolution of Model-3 with convergent boundary force of  $9.0 \times 10^{12}$  N/m, same as Figure 6a.  
 289 (b) Evolution of Model-4 with convergent boundary force of  $8.5 \times 10^{12}$  N/m, same as Figure 6b.

290

### 291 3.2.2 Existence of a prescribed weak zone at the neighboring passive margin

292 The existence of a prescribed weak zone at the passive margin dramatically reduces the  
 293 required convergent force for SI after collision. For example, the boundary force required for SI  
 294 at the neighboring passive margin with 60 Ma oceanic lithosphere is  $\sim 4.0 \times 10^{12}$  N/m (Figure 8),  
 295 which is about half of that in the models without weak zone. Two modes of SI are obtained  
 296 according to systematic numerical studies, which are the earlier SI after initial collision and the  
 297 later SI after slab break-off (Figure 8). In the models with younger oceanic plate and relatively  
 298 larger boundary force, the SI results immediately after the initial collision. In contrast with older  
 299 oceanic plate and relatively smaller boundary force, the SI occurs much later after the slab break-  
 300 off. It is worth noting that the models with very low convergent forces encounter serious  
 301 problems in the solver convergence, which thus prevents obtaining models without SI in this  
 302 regime.

303



304

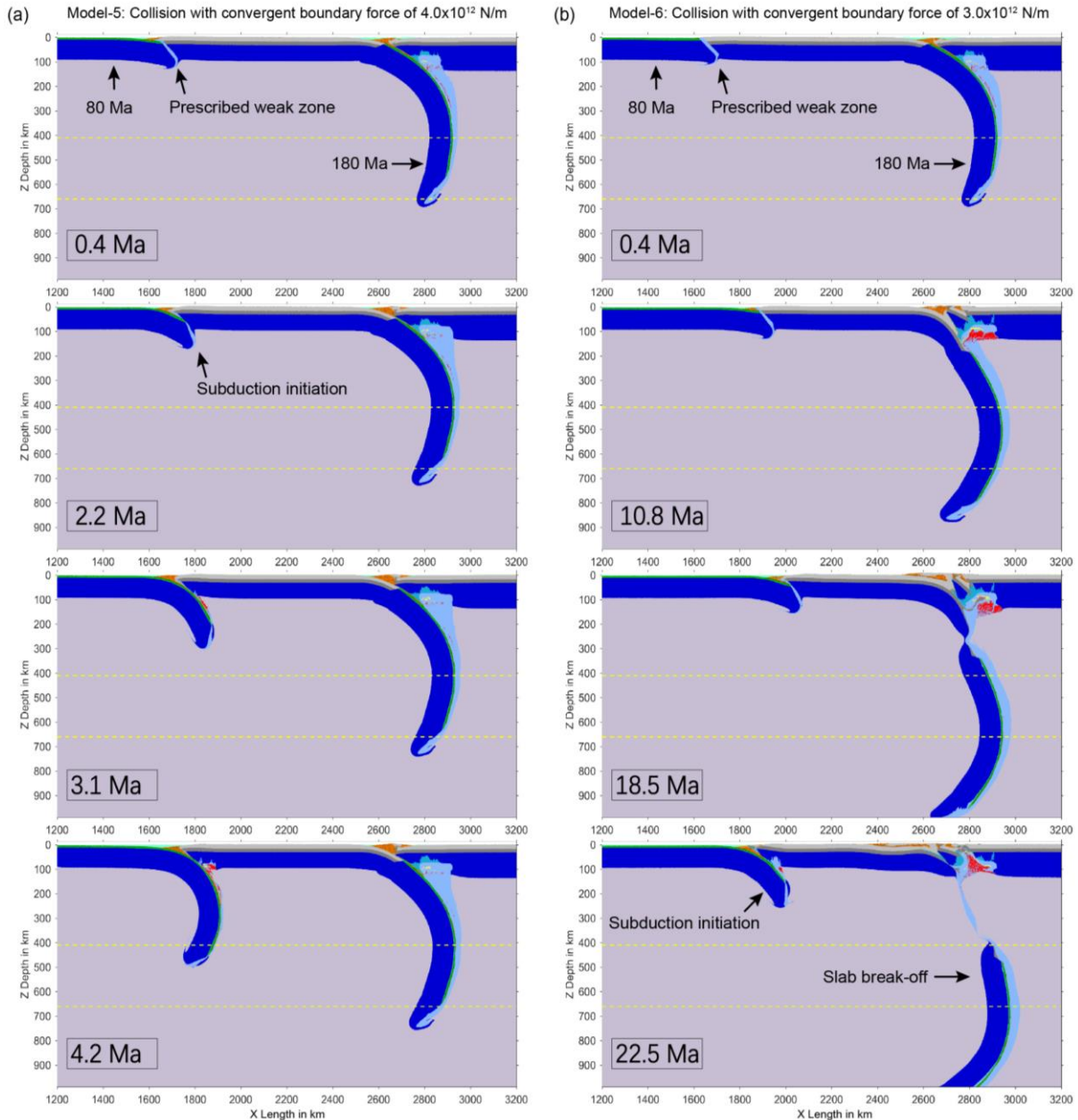
305 **Figure 8.** Two contrasting modes of forced subduction initiation (SI) at the neighboring passive  
 306 margin with a prescribed weak zone, i.e. earlier SI after initial collision versus later SI after slab  
 307 break-off, dependent on the age of oceanic lithosphere and the convergent boundary force.

308

309 The evolution of two contrasting models are demonstrated in Figures 9 and 10, which are  
 310 either SI after collision (Model-5 with oceanic lithosphere of 80 Ma and boundary force of  
 311  $4.0 \times 10^{12}$  N/m) or SI after slab break-off (Model-6 with oceanic lithosphere of 80 Ma and  
 312 boundary force of  $3.0 \times 10^{12}$  N/m).

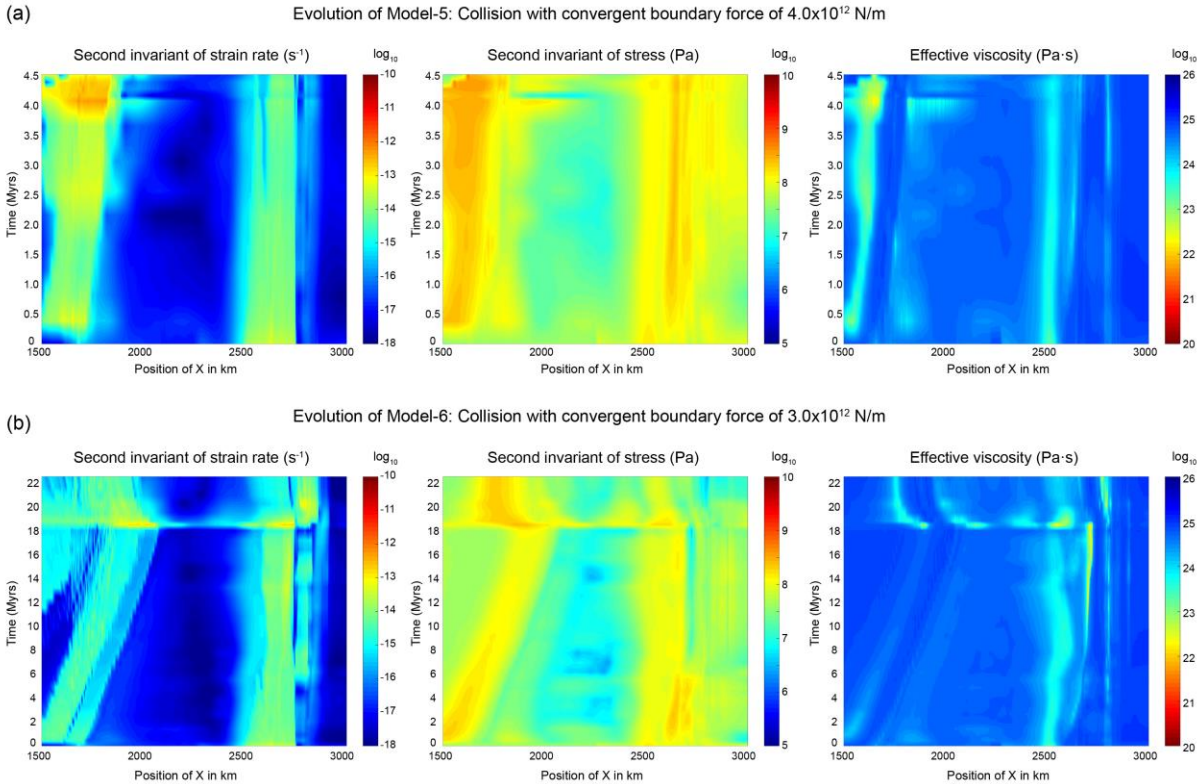
313 In Model-5, the SI occurs at the neighboring passive margin soon after the continental  
 314 collision (Figure 9a). The significant stress localization in the passive margin leads to the failure  
 315 of prescribed weak zone and the occurrence of SI (Figure 10a). The forced convergence is  
 316 accommodated by both subduction zones, i.e. the old one on the right and the newly formed one  
 317 on the left (Figure 9a). However, through the model evolution, the strain rate in the old  
 318 subduction zone decreases, whereas that in the new subduction zone increases (Figure 10a). It  
 319 indicates the dominance of convergence switches gradually from the old subduction zone to the  
 320 new one.

321 In Model-6, the relatively low convergent force is not enough to trigger SI immediately  
 322 after collision (Figure 9b). Although SI does not occur, there is still deformation localized in the  
 323 weak zone after collision, which is clearly demonstrated by the stress building and resulting  
 324 higher strain rates (Figure 10b). However, the deformation in the passive margin is too slow for  
 325 the occurrence of SI. At about 18.5 Myrs after collision, the slab break-off occurs with eduction  
 326 of continental plate, which results in an additional push on the neighboring passive margin.  
 327 Finally, the SI is induced, which is further sustained by the continuous convergent boundary  
 328 force.



329

330 **Figure 9.** Models of forced subduction initiation at the neighboring passive margin with a  
 331 prescribed weak zone, with colors indicating rock types as in Figure 2. (a) Evolution of Model-5  
 332 with convergent boundary force of  $4.0 \times 10^{12}$  N/m. (b) Evolution of Model-6 with convergent  
 333 boundary force of  $3.0 \times 10^{12}$  N/m.



334

335 **Figure 10.** The time-dependent evolution of strain rate, stress and viscosity fields. The position  
 336 of the profile ( $X = 1500\sim 3000$  km) is indicated by the red box of Figure 2b, with values of  
 337 second invariant of strain rate and stress, as well as the effective viscosity averaged with depth.  
 338 (a) Evolution of Model-5 with convergent boundary force of  $4.0 \times 10^{12}$  N/m, same as Figure 9a.  
 339 (b) Evolution of Model-6 with convergent boundary force of  $3.0 \times 10^{12}$  N/m, same as Figure 9b.

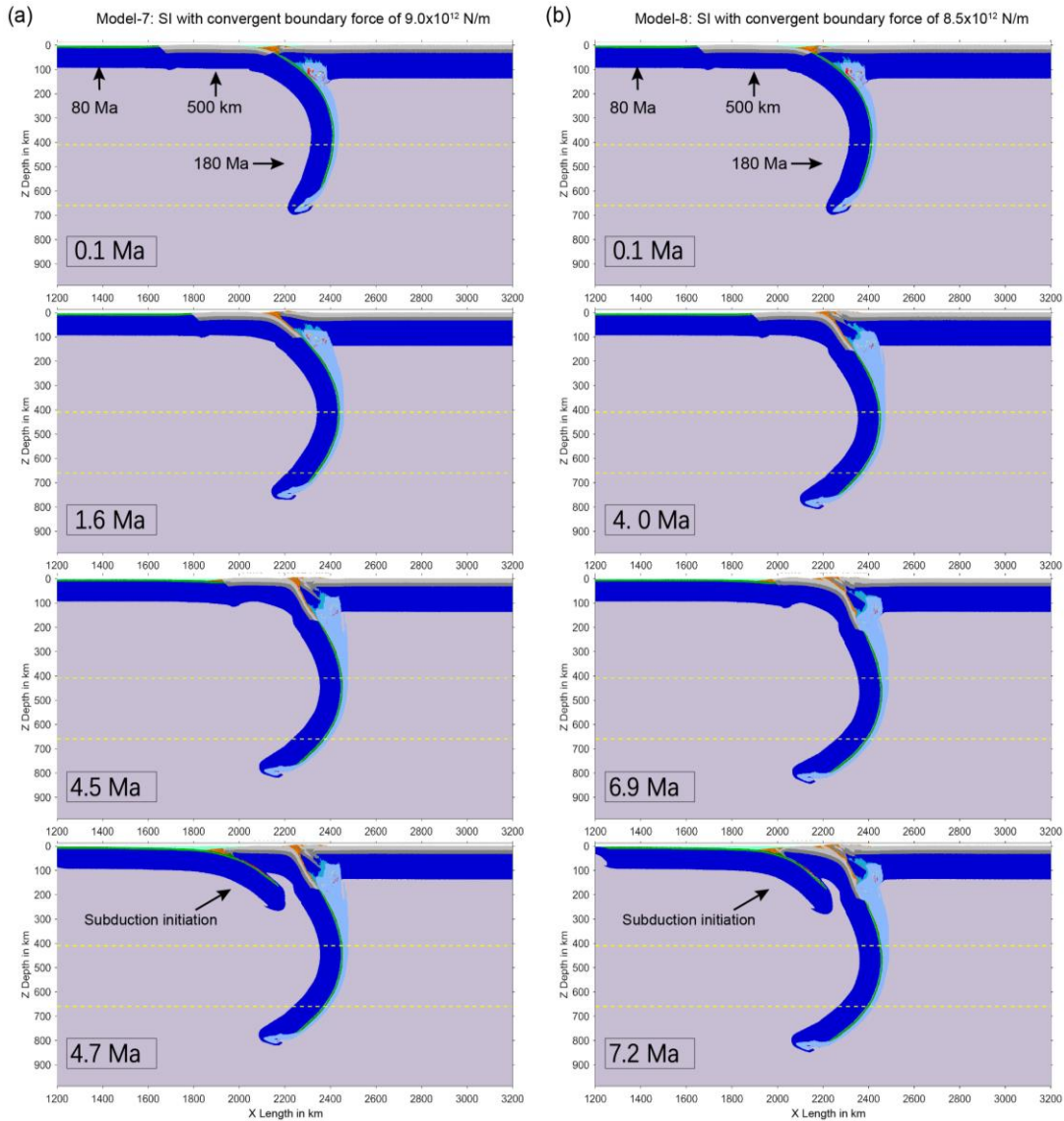
340

### 341 3.3 Effect of the length of accreted continental terrane

342 In the previous models, the length of drifting continental terrane within the subducting  
 343 oceanic plate is constant of 1000 km. During the Tethyan evolution, the multiple terranes  
 344 accreted to the Eurasian plate may be wider (e.g., Indian plate) or narrower (e.g., Lhasa terrane).  
 345 However, it is worth noting that the Lhasa terrane is included in the Cimmerian block, the length  
 346 of which is hard to constrain. In order to understand the effect of the terrane's length on the SI at  
 347 the neighboring passive margin, comparable experiments are further conducted with shorter  
 348 terrane of 500 km.

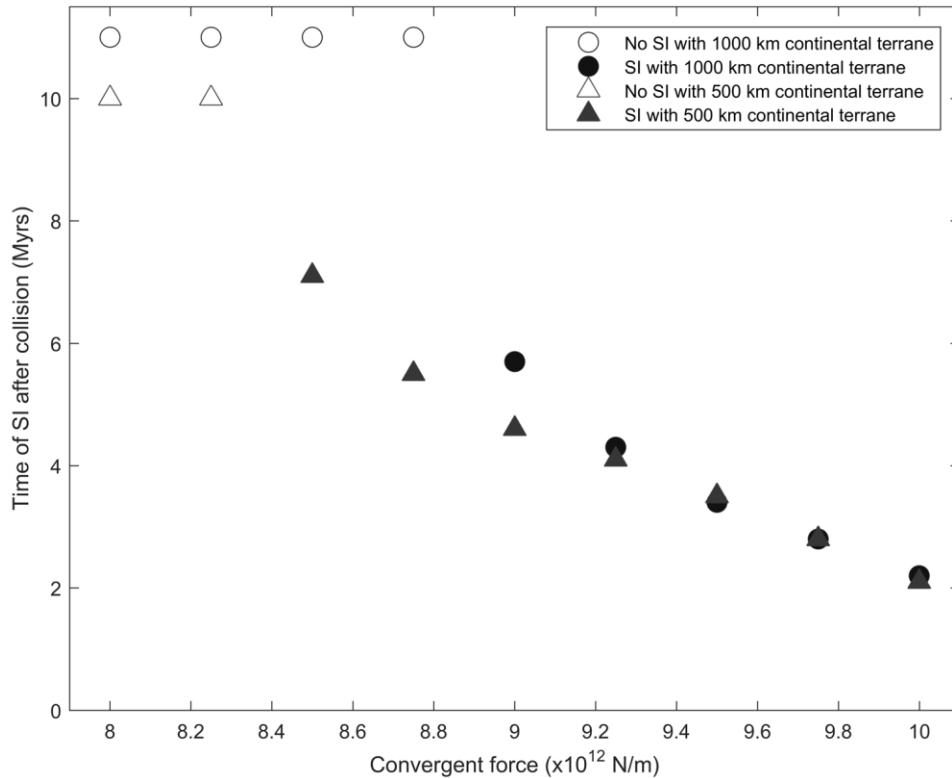
349 Model-7 and Model-8 are comparable to Model-3 (Figure 6a) and Model-4 (Figure 6b),  
 350 respectively. The only difference is the application of a shorter drifting continental terrane (500  
 351 km). The evolutions of these two additional models are similar to Model-3 (Figure 6a), in which  
 352 the SI occurs at the neighboring passive margin after the continental deep subduction (Figure  
 353 11). The comparisons between Model-8 (SI in Figure 11b) and Model-4 (no SI in Figure 6b)  
 354 indicate that the shorter drifting continental terrane favors the collision-induced subduction  
 355 transference.

356 In order to better understand the effects of continental terrane's length, we further  
 357 conduct a set of numerical models with shorter continental terrane and compare them to the  
 358 previous models with longer continental terrane (Figure 12). The results indicate that the length  
 359 of drifting continental terrane does not play significant roles in the models with higher boundary  
 360 forces. However, in the regime with lower boundary forces, the collision of a shorter continental  
 361 terrane leads to SI a bit earlier (by 0~2 Myrs) and easier (by decreasing the required boundary  
 362 force of  $0.6 \times 10^{12}$  N/m) than a longer one (Figure 12).



363  
 364 **Figure 11.** Models with shorter drifting continental terrane of 500 km, with colors indicating  
 365 rock types as in Figure 2. (a) Evolution of Model-7 with convergent boundary force of  $9.0 \times 10^{12}$   
 366 N/m, comparable to Model-3 in Figure 6a. (b) Evolution of Model-8 with convergent boundary  
 367 force of  $8.5 \times 10^{12}$  N/m, comparable to Model-4 in Figure 6b.

368



369

370 **Figure 12.** Comparisons among models with shorter (500 km) and longer (1000 km) drifting  
 371 continental terranes. The circles show the results of numerical models as in Figure 5 with  
 372 spreading oceanic plate of 80 Ma and longer continental terrane of 1000 km, whereas the  
 373 triangles for the comparable models with shorter continental terrane of 500 km. All the other  
 374 parameters are identical.

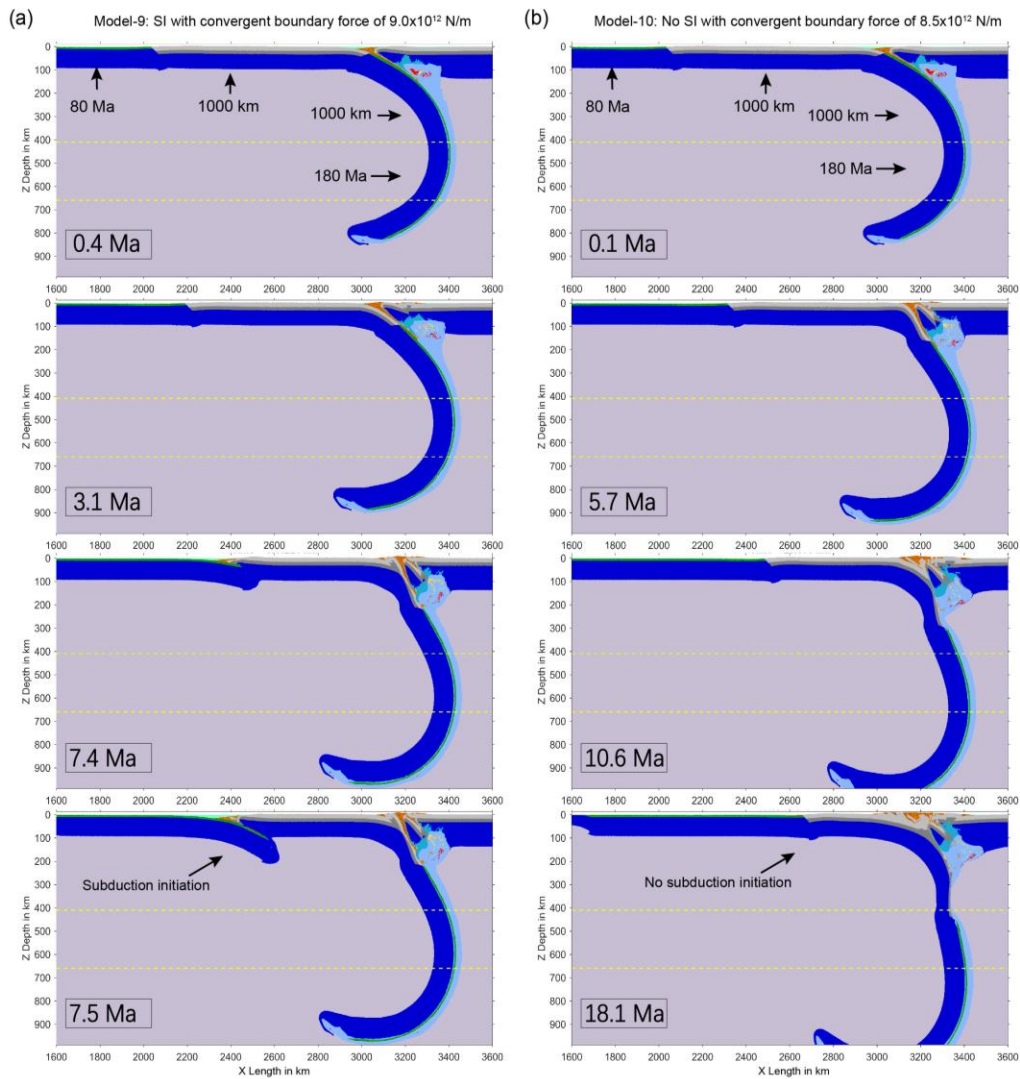
375

### 376 3.4 Effect of the length of the firstly subducted oceanic slab

377 In the previous models, the length of the firstly subducted oceanic slab is constant of 600  
 378 km, which leads to the slab arriving at around 660 km discontinuity, i.e. the boundary between  
 379 the upper and lower mantles. Further varying the length of subducted slab may play a role in  
 380 modifying the force of slab pull. In order to test its effects on the SI at the neighboring passive  
 381 margin, additional experiments are conducted with longer subducted oceanic slab of 1000 km  
 382 (Figures 13, 14).

383 In the regime with relatively lower convergent force of  $8.5 \times 10^{12}$  N/m, the evolution of  
 384 Model-10 is very similar to Model-4 although with difference lengths of subducted slab (c.f.  
 385 Figures 13b and Figure 6b). No SI is predicted at the neighboring passive margin of both models.  
 386 Alternatively, in the regime with relatively higher convergent force of  $9.0 \times 10^{12}$  N/m, the  
 387 collision-induced SI at the passive margin occurs a bit later for ~2 Myrs in Model-9 with a  
 388 longer subducted oceanic slab of 1000 km than that in Model-3 with a shorter subducted slab of  
 389 600 km (c.f. Figures 13a and Figure 6a). Figure 14 further summarizes and illustrates the effects  
 390 of subducted slab length on the time of SI at the neighboring passive margin. It indicates that the  
 391 time of SI after collision is generally later (by ~2 Myrs) in the models with a longer subducted

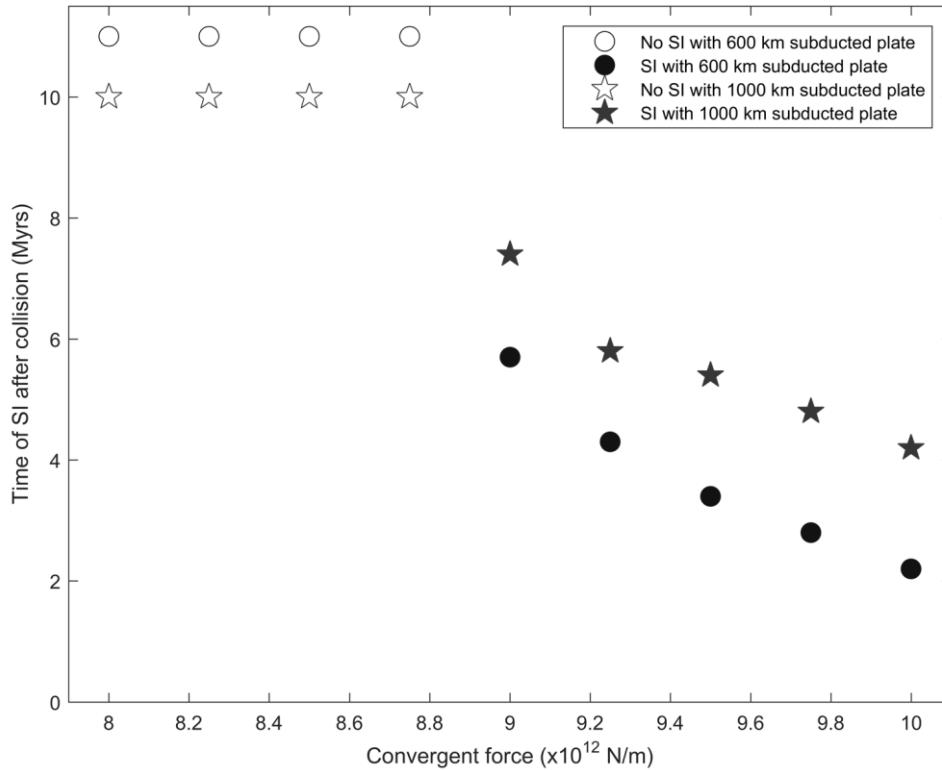
392 slab of 1000 km than those of 600 km, because the larger slab pull delays the stress building and  
 393 lithospheric collapse. However, the length of subducted slab does not affect the threshold of  
 394 convergent force required to trigger SI at the neighboring passive margin. Thus, it plays  
 395 secondary roles in the collision-induced subduction transference.



396

397 **Figure 13.** Numerical models with subducted oceanic plate of 1000 km. All the other parameters  
 398 are comparable to Model-3 and Model-4, respectively (Figure 6). The colors indicate rock types  
 399 as in Figure 2. (a) Evolution of Model-9 with convergent boundary force of  $9.0 \times 10^{12}$  N/m. (b)  
 400 Evolution of Model-10 with convergent boundary force of  $8.5 \times 10^{12}$  N/m.

401



402

403 **Figure 14.** Comparisons among models with shorter (600 km) or longer (1000 km) subducted  
 404 oceanic plate. The circles show the results of numerical models as in Figure 5 with spreading  
 405 oceanic plate of 80 Ma and subducted oceanic plate of 600 km, whereas the stars for the  
 406 comparable models with longer subducted oceanic plate of 1000 km. All the other parameters are  
 407 identical.

408

## 409 4 Discussion

### 410 4.1 Controlling factors of collision-induced subduction transference

411 The collision-induced subduction transference is a complex dynamic process, which is  
 412 affected by not only the present subduction/collision itself, but also the properties of the  
 413 neighboring passive margin and the boundary conditions. The current numerical models indicate  
 414 that the resistance of convergence from continental collision leads to stress building in the  
 415 neighboring plate and passive margin (e.g., Figures 4 and 7). On the other hand, the slab break-  
 416 off and the resulting eduction can trigger the incipient SI at the neighboring passive margin (e.g.,  
 417 Figures 3b and 9b). However, the steady SI and the final development of mature subduction  
 418 require additional forces, e.g., the boundary convergence force. In Model-2 without boundary  
 419 force (Figure 3b), the incipient SI does not evolve into a self-sustained subduction zone because  
 420 of the short and limited convergence from slab break-off. In contrast, the similarly induced SI is  
 421 sustained by the convergent force in Model-6 (Figure 9b). Thus, the convergent force on the  
 422 drifting oceanic plate is a critical factor for the occurrence of collision-induced subduction  
 423 transference. In addition, the increasing of convergent force could extensively reduce the time  
 424 for SI after collision, as shown in Figure 5.

425 The rheological strength of the passive margin is controlled by the age of neighboring  
426 oceanic lithosphere as well as the possible presence of weak zones. The numerical models  
427 indicate that the collision-induced SI at the passive margin without weak zone generally requires  
428 a high convergent force of above  $8.0 \times 10^{12}$  N/m (Figure 5). However, the force of ridge push is  
429 estimated to be around  $3.0 \times 10^{12}$  N/m (*Harper, 1975; Turcotte and Schubert, 1982; Ghosh et al.,*  
430 *2006; Mahatsente, 2017; Sun, 2019*), which is not large enough for the collision-induced SI. The  
431 existence of a weak zone with wet olivine rheology (*Karato and Wu, 1993*) at the OCT can  
432 significantly reduce the required convergent force for SI after collision (Figure 8), i.e. no higher  
433 than  $3.0 \sim 5.0 \times 10^{12}$  N/m. On the other hand, the age of the neighboring oceanic plate plays a  
434 second-order role in the collision-induced subduction transference, comparing to effects of weak  
435 zone and boundary force, although the required force for triggering SI increases slightly with the  
436 oceanic lithospheric age in both models with and without weak zones (Figures 5 and 8). The  
437 effects of oceanic age are two-folded, i.e. on viscosity and density, respectively. In the viscosity  
438 aspect, the old oceanic lithosphere increases the thickness and rheological strength of the passive  
439 margin, which leads to difficulty in its collapse and further SI. In the density aspect, the  
440 negatively buoyancy of oceanic plate increases with age and thus contributes to the gravity  
441 instability and further the SI. However, the increase of strength and resistance to SI dominates,  
442 which finally results in the positive correlation between the oceanic age and the required  
443 convergent force for SI at the neighboring passive margin (Figures 5 and 8).

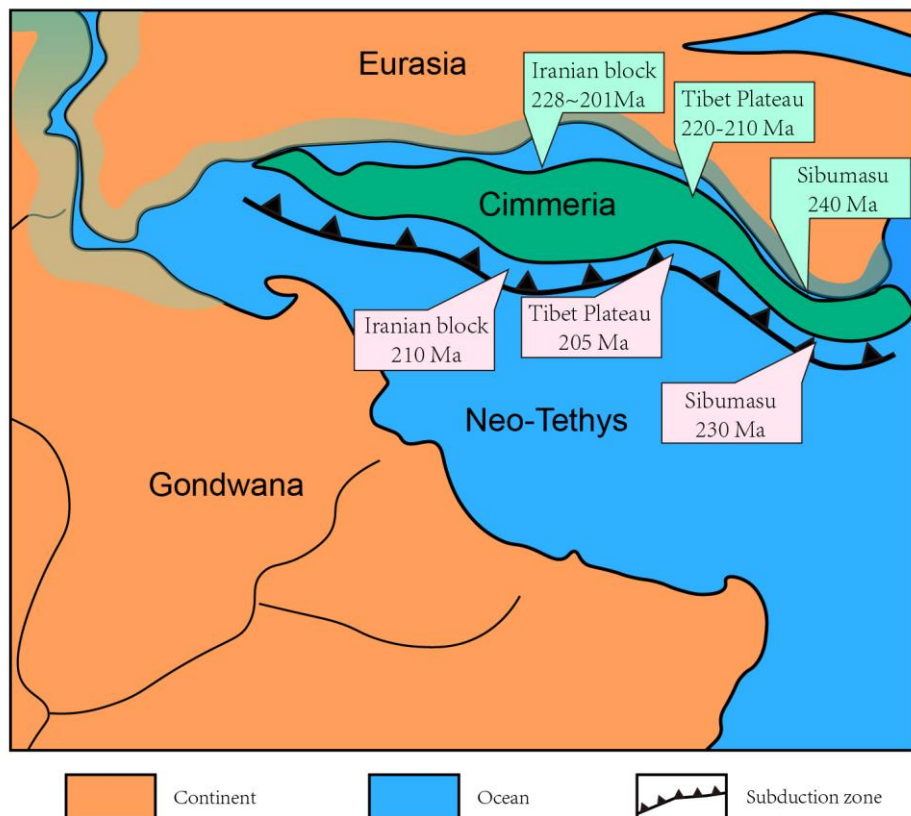
444

#### 445 **4.2 Implications for the dynamics of Tethyan evolution**

446 The Tethyan system is a large scale and long living orogenic system on the Earth since  
447 the Paleozoic. The most special and intriguing character of Tethys is the multiple terranes or  
448 microcontinents drifting from Gondwana, and accreting to the Eurasia (or Laurasia) continent  
449 (Figure 1c) (*Wan et al., 2019*). The drifting and collision processes of the Galatian  
450 supercontinent and the following SI of the Paleo-Tethys in the Early Paleozoic are much far  
451 away from present and consequently not well constrained from the geological records. Thus, we  
452 focus on the collision of the Cimmerian terranes with Eurasia and the following SI of the Neo-  
453 Tethys. More geological records can be obtained to constrain this collision-induced subduction  
454 transference.

455 The Neo-Tethyan tectonic belt is very long for  $\sim 10,000$  km from the Western Europe to  
456 the Southeastern Asia. Here we focus on the regions with relatively well constrained  
457 geochronologic data, as shown in Figure 15. In the middle Tethys, the collision of Iranian block  
458 with the Eurasia is recorded by the deformation of early Mesozoic strata in Fariman basin, which  
459 indicates the time of collision is around 228-201 Ma (*Wan et al., 2019; Zanchi et al., 2016*). The  
460 subduction of the neighboring Neo-Tethyan oceanic plate in Iranian region started at about 200  
461 Ma (*Wilmsen et al., 2009*), which was a bit later than the collision. Alternatively, for Tibetan  
462 Plateau, the collision between Cimmeria and Eurasia occurred at about 220-210 Ma, while the SI  
463 in this region was at about 205 Ma (*Wan et al., 2019; and references therein*). Further to the east,  
464 the collision between the Sibumasu and Indo-China (part of Eurasia at that time) occurred at  
465 about 240 Ma, while the SI at the neighboring Neo-Tethyan Ocean was about 230 Ma (*Metcalfe,*  
466 *2013*). As a summary, the SI of Neo-Tethys is generally following the collision of Cimmerian  
467 plates with Eurasia, with a time delay of  $< 20$  Myrs as shown in Figure 15. It is worth noting that  
468 various geological records are previously used as the proxy for the start of collision, e.g., the

469 exhumation of eclogite, the strata deformation, the metamorphic rocks, etc. Thus, the timing of  
 470 collision is a bit varied among different studies (*Yin and Harrison, 2000; Aitchison et al., 2007;*  
 471 *Najman, et al., 2010; DeCelles et al., 2014; Zhu et al., 2015; Searle, 2019*). On the other hand,  
 472 the geological records for SI are even more complex (*Stern, 2004; Stern et al., 2012; Hall, 2018;*  
 473 *Guilmette et al., 2019; Searle, 2019; Patriat et al., 2019; Parlak et al., 2019*). The emplacement  
 474 of magmatic rock is generally later, by several million years, than the exact time of SI (*Hall,*  
 475 *2018; Shervais et al., 2019; Arculus et al., 2019*). Thus, the timing of SI may be delayed  
 476 according to the magmatic records. The current numerical models indicate that the SI occurs in  
 477 the neighboring plate within 10 Myrs after collision, under the favorable conditions of collision-  
 478 induced subduction transference (Figure 5). Considering all the uncertainties as discussed above,  
 479 the numerical models are consistent with the observations in the middle-eastern Tethys (Figure  
 480 15).



481  
 482 **Figure 15.** The conceptual model of subduction transference during the collision between  
 483 Cimmerian terranes and Eurasian continent (modified after *Stampfli and Borel, 2002*). The  
 484 numbers in the blue boxes show the estimated time of collision (*Metcalfe, 2013; Zanchi et al.,*  
 485 *2016; Wan et al., 2019*), whereas those in the pink boxes indicate the time of subduction  
 486 initiation of the Neo-Tethyan oceanic plate (*Wilmsen et al., 2009; Metcalfe, 2013; Wan et al.,*  
 487 *2019*).

488  
 489 Another issue for discussion is whether and when will the SI occur in the Indian Ocean as  
 490 a response to the India-Asia collision, which is a challenging problem. The collision has already  
 491 occurred for more than about 50 Ma (*Yin and Harrison, 2000; Aitchison et al., 2007; Najman et*

492 *al.*, 2010; *Lippert, et al.*, 2014; *Zhu et al.*, 2015; *Searle*, 2019); however, there is still no clear  
493 sign for the SI to the south of Indian continent, although some guesses have been suggested (*Niu*  
494 *et al.*, 2003; *Stern*, 2004; *Stern and Gerya*, 2018; *Pandey et al.*, 2019). Several reasons have been  
495 proposed for the absence of SI in the Indian ocean, although none has been confirmed, for  
496 example, the continuous shortening of overriding Tibetan plateau, the large width or the  
497 triangular shape of the Indian plate, the strength of an old and stable OCT (*Cloetingh*, 1989;  
498 *Stern*, 2004; *Stern and Gerya*, 2018). Based on our numerical models, the difficulty for the SI in  
499 the Indian Ocean may be due to the low convergent force and/or the lack of proper weak zones at  
500 the passive margin. The convergent force between the Indian plate and the Eurasian continent is  
501 estimated by the GPE to be about  $3.0 \times 10^{12}$  N/m (*Ghosh et al.*, 2006; *Schmalholz et al.*, 2014),  
502 which is lower than the required force for triggering SI for the neighboring Indian Oceanic plate  
503 with over 100 Ma lithosphere, if no weak zone is present (Figure 5). In this case, the  
504 convergence between plates is mainly accommodated by the deformation in the Himalayan  
505 collision zone, which is consistent with Model-4 (Figure 6b). On the other hand, the absence of  
506 SI in the Indian Ocean may also be a result of lack of proper weak zone according to our  
507 numerical models. The existence of weak zone is a common case on the Earth, which could be  
508 the faults, hydration zones and highly deformed/fracture zones (*Gurnis and Hall*, 2004; *Leng and*  
509 *Gurnis*, 2011; *Zhou et al.*, 2018; *Arcay et al.*, 2019). These weak zones may not collapse into  
510 subduction zone under the typical tectonic force of ridge push of about  $3.0 \times 10^{12}$  N/m (*Turcotte*  
511 *and Schubert*, 1982; *Mahatsente*, 2017) as shown in Figure 8. However, a short but strong  
512 impulse (e.g., slab break-off) can result in an incipient subduction zone, which is then sustained  
513 by a low convergent force (e.g.,  $3.0 \times 10^{12}$  N/m) in Model-6 (Figure 9b). Obviously, the Indian  
514 plate has experienced the collision and slab break-off (*Yin and Harrison*, 2000; *Kohn and*  
515 *Parkinson*, 2002; *Aitchison et al.*, 2007; *Najman et al.*, 2010; *Zhu et al.*, 2015). The absence of SI  
516 may indicate the lack of proper weak zones in the Indian Oceanic plate to localize the incipient  
517 subduction.

518

## 519 **5. Conclusions**

520 The collision-induced subduction transference includes two aspects, i.e. the terrane  
521 collision/accretion and the subduction initiation (SI) at the neighboring passive margin, the  
522 dynamics of which are generally investigated individually. In this study, we combine these two  
523 regimes into an integrated model, and conduct systematic numerical experiments. The main  
524 conclusions include the following:

- 525 (1) The boundary force-driven convergence is required to trigger and sustain the SI at the  
526 neighboring passive margin after terrane collision and accretion. In contrast, the self-  
527 consistent force variations in the existing subduction/collision system (e.g., induced by  
528 continental subduction and/or slab break-off) are not enough for the subduction  
529 transference, although they can indeed trigger the incipient SI.
- 530 (2) The existence of weak zone at the passive margin can significantly promote the  
531 occurrence of SI, by decreasing the required boundary force to the reasonable value of  
532 plate tectonics. In addition, the age of oceanic lithosphere also plays a certain role by  
533 affecting the strength of passive margin, e.g., easier SI for younger oceanic plate under  
534 the same boundary force.
- 535 (3) The length of subducted oceanic slab or the accreting continental terrane plays secondary  
536 roles in the occurrence of SI after collision.

- 537 (4) Under the favorable conditions of collision-induced subduction transference, the time  
 538 required for SI after collision is generally short within 10 Myrs, which is strongly  
 539 dependent on the convergent boundary force, but weakly on the age of oceanic  
 540 lithosphere.
- 541 (5) The SI of the Neo-Tethyan oceanic plate generally occurred shortly after the collision  
 542 between the Cimmerian terranes and Eurasian continent, which may indicate the  
 543 relatively large convergent force and/or weakened passive margin. In contrast, the stable  
 544 Indian passive margin and absence of SI in the Indian Ocean may due to the low  
 545 convergent force and/or the lack of proper weak zones, which still requires further studies.  
 546

## 547 **Acknowledgment**

548 The research leading to these results has received funding from the NSFC Tethys project  
 549 (91855208), the Strategic Priority Research Program (B) of Chinese Academy of Sciences  
 550 (XDB18000000), the NSFC normal project (41774108), as well as the support from the  
 551 University of Chinese Academy of Sciences. Numerical simulations were run with the clusters of  
 552 National Supercomputer Center in Guangzhou (Tianhe-II). *Taras Gerya, Di-Cheng Zhu, and Bo*  
 553 *Wan* are acknowledged for the helpful discussion. The authors declare no conflict of interest. The  
 554 figures of numerical models are produced by the Matlab of MathWorks and further compiled by  
 555 the Adobe Illustrator. All related data will be provided in Zenodo (<https://doi.org/xxxxxx>).  
 556

## 557 **References**

- 558 Aitchison, J. C., Ali, J. R., & Davis, A. M. (2007). When and where did India and Asia collide? *Journal of*  
 559 *Geophysical Research: Solid Earth*, 112(B5).
- 560 Arcay, D., Lallemand, S., Abecassis, S., & Garel, F. (2019) Can subduction initiation at a transform fault be  
 561 spontaneous? *Solid Earth Discuss.*, <https://doi.org/10.5194/se-2019-63>, in review.
- 562 Arculus, R. J., Gurnis, M., Ishizuka, O., Reagan, M. K., Pearce, J. A., & Sutherland, R. (2019). HOW TO  
 563 CREATE NEW SUBDUCTION ZONES. *Oceanography*, 32(1), 160-174.
- 564 Baes, M., Govers, R., & Wortel, R. (2011). Subduction initiation along the inherited weakness zone at the edge  
 565 of a slab: Insights from numerical models. *Geophysical Journal International*, 184(3), 991-1008.
- 566 Baes, M., & Sobolev, S. V. (2017). Mantle flow as a trigger for subduction initiation: A missing element of the  
 567 Wilson Cycle concept. *Geochemistry, Geophysics, Geosystems*, 18(12), 4469-4486.
- 568 Cloetingh, S., Wortel, R., & Vlaar, N. J. (1989). On the initiation of subduction zones. In *Subduction Zones*  
 569 *Part II* (pp. 7-25). Birkhäuser Basel.
- 570 Cramer, F., Schmeling H., Golabek G. J., Duretz T., Orendt R., Buitert S., May D., Kaus B., Gerya T., &  
 571 Tackley P. (2012), A comparison of numerical surface topography calculations in geodynamic modelling:  
 572 an evaluation of the 'sticky air' method, *Geophysical Journal International*, 189, 38-54.
- 573 DeCelles, P. G., Kapp, P., Gehrels, G. E. & Ding L. (2014). Paleocene-Eocene foreland basin evolution in the  
 574 Himalaya of southern Tibet and Nepal: Implications for the age of initial India-Asia collision. *Tectonics*  
 575 33, doi: 10.1002/2014TC003522.
- 576 Duretz, T., Gerya, T. V., Kaus, B. J. P., & Andersen, T. B. (2012). Thermomechanical modeling of slab  
 577 education. *Journal of Geophysical Research: Solid Earth*, 117(B8).
- 578 Ghosh, A., Holt, W. E., Flesch, L. M., & Haines, A. J. (2006). Gravitational potential energy of the Tibetan  
 579 Plateau and the forces driving the Indian plate. *Geology*, 34(5), 321-324.
- 580 Guilmette, C., Smit, M. A., van Hinsbergen, D. J., Gürer, D., Corfu, F., Charette, B., ... & Savard, D. (2018).  
 581 Forced subduction initiation recorded in the sole and crust of the Semail Ophiolite of Oman. *Nature*  
 582 *Geoscience*, 11(9), 688.

- 583 Gurnis, M., Hall, C. E., & Lavier, L. L. (2004), Evolving force balance during incipient subduction,  
584 *Geochemistry Geophysics Geosystems*, 5(7).
- 585 Hall, R. (2018), The subduction initiation stage of the Wilson cycle, Geological Society, London, Special  
586 Publications.
- 587 Harper, J. F. (1975). On the driving forces of plate tectonics. *Royal Astronomical Society Geophysical Journal*,  
588 40, 465–474.0.
- 589 Karato, S., & Wu, P. (1993). Rheology of the upper mantle: A synthesis. *Science*, 260(5109), 771–778.
- 590 Kohn, M. & Parkinson, C. D. (2002). Petrologic case for Eocene slab breakoff during the Indo-Asian collision.  
591 *Geology* 30, 591–594.
- 592 Leng, W., & Gurnis, M. (2011). Dynamics of subduction initiation with different evolutionary pathways.  
593 *Geochemistry, Geophysics, Geosystems*, 12(12).
- 594 Li, Z.-H., Gerya, T., & Connolly, J. A. D. (2019). Variability of subducting slab morphologies in the mantle  
595 transition zone: Insight from petrological-thermomechanical modeling. *Earth-Science Reviews*, 196,  
596 102874.
- 597 Lippert, P. C., van Hinsbergen, D. J. J. & Dupont-Nivet, G. (2014). Early Cretaceous to present latitude of the  
598 central proto-Tibetan Plateau: A paleomagnetic synthesis with implications for Cenozoic tectonics,  
599 paleogeography, and climate of Asia. *Geological Society of America Special Papers*, 507, 1–21.
- 600 Mahatsente, R. (2017). Global models of ridge-push force, geoid, and lithospheric strength of oceanic plates.  
601 *Pure and Applied Geophysics*, 174(12), 4395-4406.
- 602 Marques, F. O., Cabral, F. R., Gerya, T. V., Zhu, G., & May, D. A. (2014). Subduction initiates at straight  
603 passive margins. *Geology*, 42(4), 331–334.
- 604 Marques, F. O., Nikolaeva, K., Assumpção, M., Gerya, T. V., Bezerra, F. H. R., do Nascimento, A. F., &  
605 Ferreira, J. M. (2013). Testing the influence of far-field topographic forcing on subduction initiation at a  
606 passive margin. *Tectonophysics*, 608, 517 - 524. <https://doi.org/10.1016/j.tecto.2013.08.035>
- 607 Mason, W. G., Moresi, L., Betts, P. G., & Miller, M. S. (2010). Three-dimensional numerical models of the  
608 influence of a buoyant oceanic plateau on subduction zones. *Tectonophysics*, 483(1-2), 71-79.
- 609 Metcalfe, I. (2013). Gondwana dispersion and Asian accretion: Tectonic and palaeogeographic evolution of  
610 eastern Tethys. *Journal of Asian Earth Sciences*, 66, 1-33.
- 611 Mueller, S., & Phillips, R. J. (1991). On the initiation of subduction. *Journal of Geophysical Research: Solid*  
612 *Earth*, 96(B1), 651-665.
- 613 Müller, R. D., Sdrolias, M., Gaina, C., & Roest, W. R. (2008). Age, spreading rates and spreading symmetry of  
614 the world's ocean crust. *Geochemistry, Geophysics, Geosystems*, 9, Q04006.  
615 <https://doi.org/10.1029/2007GC001743>.
- 616 Najman, Y., Appel, E., Boudagherfadel, M. K., Bown, P. R., Carter, A., Garzanti, E., ... & Vezzoli, G. (2010).  
617 Timing of India - Asia collision: Geological, biostratigraphic, and palaeomagnetic constraints. *Journal of*  
618 *Geophysical Research*, 115, B12416, doi: 10.1029/2010JB007673.
- 619 Nikolaeva, K., Gerya, T. V., & Marques, F. O. (2011). Numerical analysis of subduction initiation risk along  
620 the Atlantic American passive margins. *Geology*, 39(5), 463-466.
- 621 Niu, Y., O'Hara, M. J., & Pearce, J. A. (2003). Initiation of subduction zones as a consequence of lateral  
622 compositional buoyancy contrast within the lithosphere: a petrological perspective. *Journal of Petrology*,  
623 44(5), 851-866.
- 624 Pandey, D. K., Pandey, A., & Whattam, S. A. (2019). Relict subduction initiation along a passive margin in the  
625 northwest Indian Ocean. *Nature communications*, 10(1), 2248.
- 626 Parlak, O., Dunkl, I., Karaođlan, F., Kusky, T. M., Zhang, C., Wang, L., ... & Şimşek, G. (2019). Rapid  
627 cooling history of a Neotethyan ophiolite: Evidence for contemporaneous subduction initiation and  
628 metamorphic sole formation. *Geological Society of America Bulletin*.
- 629 Patriat, M., Falloon, T., Danyushevsky, L., Collot, J., Jean, M. M., Hoernle, K., ... & Feig, S. T. (2019).  
630 Subduction initiation terranes exposed at the front of a 2 Ma volcanically-active subduction zone. *Earth*  
631 *and Planetary Science Letters*, 508, 30-40.
- 632 Rey, P. F., Coltice, N., & Flament, N. (2014). Spreading continents kick-started plate tectonics. *Nature*,  
633 513(7518), 405.
- 634 Searle, M. P. (2019). Timing of subduction initiation, arc formation, ophiolite obduction and India–Asia  
635 collision in the Himalaya. *Geological Society, London, Special Publications*, 483(1), 19-37.

- 636 Selzer, C., Buitter, S. J., & Pfiffner, O. A. (2008). Numerical modeling of frontal and basal accretion at  
637 collisional margins. *Tectonics*, 27(3).
- 638 Şengör, A. M. C., Altner, D., Cin, A., Ustaömer, T., & Hsü, K. J. (1988). Origin and assembly of the  
639 Tethyside orogenic collage at the expense of Gondwana Land. Geological Society, London, Special  
640 Publications, 37(1), 119-181.
- 641 Shervais, J. W., Reagan, M., Haugen, E., Almeev, R. R., Pearce, J. A., Prytulak, J., ... & Li, H. (2019).  
642 Magmatic Response to Subduction Initiation: Part 1. Fore - arc Basalts of the Izu - Bonin Arc From  
643 IODP Expedition 352. *Geochemistry, Geophysics, Geosystems*, 20(1), 314-338.
- 644 Schmalholz, S. M., Medvedev, S., Lechmann, S. M., & Podladchikov, Y. (2014). Relationship between  
645 tectonic overpressure, deviatoric stress, driving force, isostasy and gravitational potential energy.  
646 *Geophysical Journal International*, 197(2), 680-696.
- 647 Schmeling, H., Babeyko, A. Y., Enns, A., Faccenna, C., Funiciello, F., Gerya, T., ... & Schmalholz, S. M.  
648 (2008). A benchmark comparison of spontaneous subduction models—Towards a free surface. *Physics of  
649 the Earth and Planetary Interiors*, 171(1-4), 198-223.
- 650 Stampfli, G. M., & Borel, G. D. (2002). A plate tectonic model for the Paleozoic and Mesozoic constrained by  
651 dynamic plate boundaries and restored synthetic oceanic isochrons. *Earth and Planetary Science Letters*,  
652 196(1-2), 17-33.
- 653 Stampfli, G. M., Hochard, C., Vérard, C., & Wilhem, C. (2013). The formation of Pangea. *Tectonophysics*,  
654 593, 1-19.
- 655 Stern, R. J., & Gerya, T. V. (2018). Subduction initiation in nature and models: A review, *Tectonophysics*,  
656 173-198.
- 657 Stern, R. J. (2017). Subduction initiation and terrane accretion, Geological Society of America Abstracts with  
658 Program. Vol. 49, No. 6. doi: 10.1130/abs/2017AM-298141.
- 659 Stern, R. J., Reagan, M., Ishizuka, O., Ohara, Y., & Whattam, S. (2012). To understand subduction initiation,  
660 study forearc crust: To understand forearc crust, study ophiolites. *Lithosphere*, 4(6), 469-483.
- 661 Stern, R. J. (2004). Subduction initiation: spontaneous and induced, *Earth and Planetary Science Letters*,  
662 226(3), 275-292.
- 663 Sun, W. (2019). The Magma Engine and subduction initiation. *Acta Geochimica*, 38(5), 611-612.  
664 <https://doi.org/10.1007/s11631-019-00366-6>
- 665 Tetreault, J. Á., & Buitter, S. J. H. (2012). Geodynamic models of terrane accretion: Testing the fate of island  
666 arcs, oceanic plateaus, and continental fragments in subduction zones. *Journal of Geophysical Research:  
667 Solid Earth*, 117(B8).
- 668 Turcotte D. L. & Schubert E. R. (1982). *Geodynamics: Applications of continuum mechanics to geological  
669 problems*, Wiley, New York.
- 670 Turcotte, D.L., & Schubert G. (2002), *Geodynamics*, Cambridge University Press, Cambridge, UK.
- 671 Ulvrova, M. M., Coltice, N., Williams, S., & Tackley, P. J. (2019). Where does subduction initiate and cease?  
672 A global scale perspective. *Earth and Planetary Science Letters*, 528, 115836.
- 673 van Hunen, J., van den Berg, A.P., & Vlaar, N.J., (2002). On the role of subducting oceanic plateaus in the  
674 development of shallow flat subduction. *Tectonophysics* 352, 317–333.
- 675 van Hunen, J., van den Berg, A. P., & Vlaar, N. J. (2004). Various mechanisms to induce present-day shallow  
676 flat subduction and implications for the younger Earth: a numerical parameter study. *Physics of the Earth  
677 and Planetary Interiors*, 146(1-2), 179-194.
- 678 Vogt, K., & Gerya, T. V. (2014). From oceanic plateaus to allochthonous terranes: numerical modelling.  
679 *Gondwana Research*, 25(2), 494-508.
- 680 Wan, B., Wu, F., Chen, L., Zhao, L., Liang, X., Xiao, W., & Zhu, R. (2019). Cyclical one-way continental  
681 rupture-drift in the Tethyan evolution: Subduction-driven plate tectonics. *Science China Earth Sciences*,  
682 1-12.
- 683 Wilmsen, M., Fürsich, F. T., Seyed-Emami, K., Majidifard, M. R., & Taheri, J. (2009). The Cimmerian  
684 Orogeny in northern Iran: Tectono-stratigraphic evidence from the foreland. *Terra Nova*, 21(3), 211-218.
- 685 Yang, S. H., Li, Z.-H., Gerya, T., Xu, Z. Q., & Shi, Y. L. (2018). Dynamics of terrane accretion during  
686 seaward continental drifting and oceanic subduction: Numerical modeling and implications for the  
687 Jurassic crustal growth of the Lhasa Terrane, Tibet. *Tectonophysics*, 746, 212-228.

- 688 Yin, A., & Harrison, T. M. (2000). Geologic evolution of the Himalayan-Tibetan orogen. *Annual review of*  
 689 *earth and planetary sciences*, 28(1), 211-280.
- 690 Zanchi A, Zanchetta S, Balini M, & Ghassemi M R. (2016). Oblique convergence during the Cimmerian  
 691 collision: Evidence from the Triassic Aghdarband Basin, NE Iran. *Gondwana Research*, 38: 149–170.
- 692 Zhong, X., & Li, Z.-H. (2019). Forced subduction initiation at passive continental margins: Velocity - driven v  
 693 ersus stress-driven. *Geophysical Research Letters*, 46, 11,054–11,064. <https://doi.org/10.1029/2019GL08>  
 694 4022.
- 695 Zhou, X., Li, Z. H., Gerya, T. V., Stern, R. J., Xu, Z., & Zhang, J. (2018). Subduction initiation dynamics  
 696 along a transform fault control trench curvature and ophiolite ages. *Geology*, 46(7), 607–610.
- 697 Zhu, D.C., Mo, X.X., Niu, Y.L., Zhao, Z.D., Wang, L.Q., Liu, Y.S., & Wu, F.Y. (2009). Geochemical  
 698 investigation of Early Cretaceous igneous rocks along an east–west traverse throughout the central Lhasa  
 699 Terrane, Tibet. *Chemical Geology* 268, 298–312.
- 700 Zhu, D. C., Zhao, Z. D., Niu, Y., Mo, X. X., Chung, S. L., Hou, Z. Q., ... & Wu, F. Y. (2011). The Lhasa  
 701 Terrane: record of a microcontinent and its histories of drift and growth. *Earth and Planetary Science*  
 702 *Letters*, 301(1-2), 241-255.
- 703 Zhu, D. C., Zhao, Z. D., Niu, Y., Dilek, Y., Hou, Z. Q., & Mo, X. X. (2013). The origin and pre-Cenozoic  
 704 evolution of the Tibetan Plateau. *Gondwana Research*, 23(4), 1429-1454.
- 705 Zhu, D. C., Wang, Q., Zhao, Z. D., Chung, S. L., Cawood, P. A., Niu, Y., ... & Mo, X. X. (2015). Magmatic  
 706 record of India-Asia collision. *Scientific Reports*, 5, 14289.
- 707
- 708

## 709 **References in Supporting Information**

- 710 Bina, C. R., & Helffrich, G. (1994). Phase transition Clapeyron slopes and transition zone seismic  
 711 discontinuity topography. *Journal of Geophysical Research: Solid Earth*, 99(B8), 15853-15860.
- 712 Bittner, D., & Schmeling, H. (1995). Numerical modelling of melting processes and induced diapirism in the  
 713 lower crust. *Geophysical Journal International*, 123(1), 59-70.
- 714 Clauser, C., & Huenges, E. (1995). Thermal conductivity of rocks and minerals. *Rock physics and phase*  
 715 *relations: a handbook of physical constants*, 3, 105-126.
- 716 Connolly, J. A. (2005). Computation of phase equilibria by linear programming: a tool for geodynamic  
 717 modeling and its application to subduction zone decarbonation. *Earth and Planetary Science Letters*,  
 718 236(1-2), 524-541.
- 719 Connolly, J. A. D. (2009). The geodynamic equation of state: what and how. *Geochemistry, Geophysics,*  
 720 *Geosystems*, 10(10).
- 721 Dziewonski, A. M., & Anderson, D. L. (1981). Preliminary reference Earth model. *Physics of the earth and*  
 722 *planetary interiors*, 25(4), 297-356.
- 723 Gerya, T.V. (2010). *Introduction to numerical geodynamic modelling*, Cambridge University Press,  
 724 Cambridge, UK.
- 725 Gerya, T. V., & Meilick, F. I. (2011). Geodynamic regimes of subduction under an active margin: effects of  
 726 rheological weakening by fluids and melts. *Journal of Metamorphic Geology*, 29(1), 7-31.
- 727 Gorczyk, W., Willner, A. P., Gerya, T. V., Connolly, J. A., & Burg, J. P. (2007). Physical controls of  
 728 magmatic productivity at Pacific-type convergent margins: Numerical modelling. *Physics of the Earth and*  
 729 *Planetary Interiors*, 163(1-4), 209-232.
- 730 Ito, K., & Kennedy G. (1971). An experimental study of the basalt-garnet granulite-eclogite transition, in:  
 731 Heacock J.G. (eds.), *The Structure and Physical Properties of the Earth's Crust*, Geophysical Monograph  
 732 Series, 14, 303-314, AGU, Washington D.C., USA.
- 733 Ito, E., & Takahashi, E. (1989). Postspinel transformations in the system Mg<sub>2</sub>SiO<sub>4</sub> - Fe<sub>2</sub>SiO<sub>4</sub> and some  
 734 geophysical implications. *Journal of Geophysical Research: Solid Earth*, 94(B8), 10637-10646.
- 735 Ito, E., Akaogi M., Topor L., & Navrotsky A. (1990). Negative pressure-temperature slopes for reactions  
 736 forming MgSiO<sub>3</sub> perovskite from calorimetry, *Science*, 249, 1275-1278.

- 737 Ito, K., & Kennedy G. (2013). An experimental study of the basalt-garnet granulite-eclogite transition, in:  
738 Heacock, J.G. (Ed.), *The Structure and Physical Properties of the Earth's Crust*, American Geophysical  
739 Union, Washington, DC.
- 740 Kameyama, M., Yuen, D. A., & Karato, S. I. (1999). Thermal-mechanical effects of low-temperature plasticity  
741 (the Peierls mechanism) on the deformation of a viscoelastic shear zone. *Earth and Planetary Science*  
742 *Letters*, 168(1-2), 159-172.
- 743 Karato, S., Riedel M., & Yuen D.A. (2001). Rheological structure and deformation of subducted slabs in the  
744 mantle transition zone: Implications for mantle circulation and deep earthquakes. *Physics of the Earth and*  
745 *Planetary Interiors*, 127, 83-108.
- 746 Katsura, T., & Ito E. (1989). The System  $Mg_2SiO_4$ - $Fe_2SiO_4$  at High Pressures and Temperatures: Precise  
747 Determination of Stabilities of Olivine, Modified Spinel, and Spinel, *Journal of Geophysical Research:*  
748 *Solid Earth*, 94(B11), 15663-15670.
- 749 Katz, R.F., Spiegelman M., & Langmuir C.H. (2003). A new parameterisation of hydrous mantle melting,  
750 *Geochemistry, Geophysics, Geosystems*, 4, 1073.
- 751 Kirby, S.H., & Kronenberg A.K. (1987). Rheology of the lithosphere: selected topics, *Reviews of Geophysics*,  
752 25, 1219-1244.
- 753 Li, Z.-H., Liu M., & Gerya T. (2016). Lithosphere delamination in continental collisional orogens: A  
754 systematic numerical study, *Journal of Geophysical Research: Solid Earth*, 121, 5186-5211.
- 755 Peacock S.M. (1990), Fluid processes in subduction zones, *Science*, 248, 329-337.
- 756 Ranalli, G. (1995). *Rheology of the earth, deformation and flow process in geophysics and geodynamics* (2nd  
757 ed.), Chapman & Hall, London, UK.
- 758 Rubie, D. C., & Ross II, C. R. (1994). Kinetics of the olivine-spinel transformation in subducting lithosphere:  
759 Experimental constraints and implications for deep slab processes. *Physics of the Earth and Planetary*  
760 *Interiors*, 86(1-3), 223-243.
- 761 Schmidt, M. W., & Poli, S. (1998). Experimentally based water budgets for dehydrating slabs and  
762 consequences for arc magma generation. *Earth and Planetary Science Letters*, 163(1-4), 361-379.
- 763